Title
Finite Element Modeling of a Model-Scale, Rock-Socketed Pile Under Cyclic Lateral Loading

Author
Bajaj, Aditya Sunil

Publication Date
2018

Peer reviewed|Thesis/dissertation

UNIVERSITY OF CALIFORNIA,
IRVINE

Finite Element Modeling of a Model-Scale, Rock-Socketed Pile under Cyclic Lateral Loading

THESIS

submitted in partial satisfaction of the requirements for the degree of

MASTER OF SCIENCE

in Civil Engineering

By

Aditya Sunil Bajaj

Thesis Committee:

Professor Anne Lemnitzer, Chair

Professor Lizhi Sun

Professor John Turner

2018

DEDICATION

To the Almighty,

My Parents

My Sister

TABLE OF CONTENTS

LIST OF FIGURES ..... **v**

LIST OF TABLES ..... **vii**

ACKNOWLEDGMENTS ..... **viii**

ABSTRACT OF THE THESIS ..... **ix**

1 INTRODUCTION **1**

1.1 Problem Statement and Objectives 1

1.2 Structural Representation of Tip Fixity 2

1.3 Modeling Approaches and Inherent Design Challenges 4

1.4 Thesis Structure 5

2 LITERATURE REVIEW **7**

2.1 General Review of Common Modelling Approaches 7

2.1.1 The subgrade reaction method 7

2.1.2 Elastic continuum approach 9

2.2 Review of Field Tests on Laterally-Loaded Pile Foundations in Rock 10

2.2.1 Frantzen and Stratton (1987) 10

2.2.2 Dykeman and Valsangkar (1996) 12

2.2.3 Reese (1997) 12

2.2.4 Gabr et al. (2002) 14

2.2.5 Yang (2006) 17

2.2.6 Parsons et al. (2010) 20

2.2.7 Guo and Lehane (2016) 23

2.3 Brief Overview of Analytical Studies 25

2.3.1 Zhang and Einstein (2000) 25

2.3.2 Vu (2006) 27

2.4 Finite Element Studies 27

2.4.1 Brown & Shie (1990) 28

2.4.2 Liang et al. (2009) 29

2.4.3. Yuan et al. (2014) 30

2.4.4 Arduino et al. (2014) 31

2.4.5 Other FEM Studies 32

3 NUMERICAL MODELLING EXERCISE 33
3.1 Brief Overview of the Numerical Model Developed by Yang et al. (2006) 33
3.2 Exercise ABAQUS Model 35
3.2.1 Geometry and Material Properties 35
3.2.2 Boundary conditions, Interactions & Loads 37
3.2.3 Mesh 38
3.3 Comparison of results 39
4 SUMMARY OF EXPERIMENTAL STUDY 43
4.1 Test Specimen and Test Setup 43
4.2 Material Properties 45
4.3 Instrumentation 45
4.4 Load Application 46
4.5 Test Results 48
5 NUMERICAL SIMULATION OF MODEL SCALE EXPERIMENT 52
5.1 Model Description and Geometry 52
5.1.1 Model boundary conditions and component interaction 53
5.1.2 Mesh 54
5.2 Material Model Parameters (Constitutive Relationships) 56
5.2.1 Soil Model 56
5.2.2 Concrete Damaged Plasticity Model 57
5.2.3 Steel Model 59
5.3 Load application and loading protocol 60
5.4 Results of FEM Analysis 62
5.4.1 Pile deflection profiles 62
5.4.2 Shear and Moment profiles 63
5.4.3 Stresses in model components 64
5.4.4 Plastic hinge development 67
5.4.5 Comparison of experiment and numerical head load displacement relationship 68
6 SUMMARY AND RECOMMENDATIONS 70
REFERENCES 74

LIST OF FIGURES

Figure 1-1 Pile soil models - representation of pile embedment 3
Figure 2-1 $p-$ y derivation procedure from field curvature measurement (Courtesy: www.FindaPile.com) 8
Figure 2-2 Subgrade reaction model based on $p-y$ curve: (a) Elevation view; (b) Elastic line; (c) p-y curves (taken from Reese 1997)..... 8
Figure 2-3 Proposed bilinear $p-y$ curves for sandstone & sandy shale (i.e., strong and unweathered rock), (reproduced after Frantzen and Stratton, 1987) 11
Figure 2-4 (a) Proposed p-y curve for weak rock (Reese 1997) (b) Simplified bilinear curve for rock (taken from Ensoft Inc. 2004)..... 14
Figure 2-5 Shaft layout for NCDOT testing (Figure taken from Gabr et al., 2002)..... 15
Figure 2-6 Instrumentation and Load test setup at Pomeroy-Mason test (Liang et al. 2009)..... 18
Figure 2-7 Instrumentation and test setup at the Dayton site (Yang, 2006) 19
Figure 2-8 Schematic of the test setup configuration at Pinjar, Australia (Guo and Lehane, 2016) 24
Figure 2-9 Shaft-Soil-Rock System with varying Elastic Modulus..... 26
Figure 2-10 View of Three-dimensional mesh with pile displaced laterally, (Brown & Shie, 1990) 29
Figure 2-11 Load vs. displacement (a) Von Mises model (b) Extended Drucker-Prager model (Brown & Shie, 1990)..... 29
Figure 2-12 Failure curves for shafts in North Carolina and Numerical tests (Yuan et al. 2014) 31
Figure 3-1 Schematic diagram of FEM model for Dayton Test validation, Yang (2006)..... 35
Figure 3-2 Mohr's Circle with linear failure envelope..... 36
Figure 3-3 ABAQUS load protocol for exercise model 38
Figure 3-4 Part meshes & element type for exercise model 39
Figure 3-5 Soil Section View: Initial Lateral stress before application of lateral load..... 40
Figure 3-6 Section view: Final lateral stress distribution at end of lateral loading 40
Figure 3-7 Pile Deflection profile for field test and ABAQUS models developed by Yang (2006) and in this study for lateral load levels of 3130kN and 5000kN 42
Figure 4-1 Experiment Setup for model scale test (Elevation View) 44

Figure 4-2 Experiment setup for model scale test (Plan View) 44
Figure 4-3 Instrumentation plan for model scale test at UC Irvine 46
Figure 4-4 (a)Displacement and (b)Force Time history (normalized time) 48
Figure 4-5 Cyclic response of test pile 49
Figure 4-6 Maximum Pile head deflection and sand surface displacement 50
Figure 4-7 Prominent Crack and Plastic Hinge location in Test pile 50
Figure 4-8 Absence of cracks in rock at interface of soils 51
Figure 5-1 Model Geometry Description 53
Figure 5-2 Pile & Soil mesh details 55
Figure 5-3 Reinforcement Meshes: Linear T3D2 elements 55
Figure 5-4 Layered Soil Profile 57
Figure 5-5 Kinematic hardening model - Stress components for tested steel material with two backstresses (Wen, 2012) 59
Figure 5-6 Reference Point for Pile Lateral Loading 61
Figure 5-7 (a) Pile head displacement for ABAQUS input and (b) Resulting Force time histories 62
Figure 5-8 Pile Deflection Profile from FEM analysis 63
Figure 5-9 Shear & Moment profile from FEM analysis at various head deflections up to 2.5cm. 64
Figure 5-10 Section view of Pile Stresses under different pile head deflection 65
Figure 5-11 Stresses in steel reinforcement at different pile head deflections 66
Figure 5-12 Stresses in sand and rock layers at different pile head deflections 66
Figure 5-13 Stress profile in Rock & Sand near pile boundary 67
Figure 5-14 Plastic Hinge Zone: Comparison of Test Specimen & FEM analysis 68
Figure 5-15 Force-Displacement comparison of experimental data and FEM analysis up to 10% pile diameter displacement 69
Figure 5-16 Overall Force-Displacement comparison of experimental data and FEM analysis 69

LIST OF TABLES

Table 2-1 Test location and rock characteristics reported by Frantzen and Stratton, 1987 11
Table 2-2 Summary of North Carolina field test geometries and results after Gabr et al. (2002) 16
Table 2-3 Summary of lateral load tests in Ohio 19
Table 2-4 Summary of shaft tests at Wyandotte County, Kansas 21
Table 2-5 LPILE Modelling parameters (Parsons et al. 2010) 22
Table 3-1 Part and Material Parameters for Dayton test site (Yang, 2006) 34
Table 3-2 Part & Material description for Assessment study 36
Table 4-1 Displacement Levels for the test specimen (δy=0.75in.) 47
Table 5-1 Elastic Material Properties of Analysis model 56
Table 5-2 Soil Plasticity Parameters 57
Table 5-3 Concrete Damaged Plasticity Parameters used in FEM Modelling (Jankowiak & Lodygowski, 2005) 58
Table 5-4 Reinforcement steel material modelling parameters 60

ACKNOWLEDGMENTS

I wish to extend my sincerest gratitude and appreciation to my advisor Dr. Anne Lemnitzer for her continuous support, guidance and constructive criticism throughout my work. Her constant encouragement towards the subject was very motivating. It was a great learning experience to be her student.

I would like to thank my thesis committee, Dr. John Turner and Dr. Lizhi Sun for their time, willingness and advise during this research work.

Special thanks to Lohrasb Keykhosropour for his assistance and direction at all stages of my work. I would also like to thank Camilla Faveretti, Dr. Bidjan Ghahreman and my colleagues in the research group for their help whenever needed.

Lastly, I would like to thank my close friends Matthew Brand, Mustafa Onur Önen, Sara Newsome and all other friends at UC Irvine for their personal support throughout the period of my master's program.

ABSTRACT OF THE THESIS

Finite Element Modeling of a Model-Scale, Rock-Socketed Pile under Cyclic Lateral Loading

By

Aditya S Bajaj

Master of Science in Civil Engineering

University of California, Irvine 2018

Professor Anne Lemnitzer, Chair

Pile foundations are extensively used in the construction of various types of superstructures, including tall buildings, bridges, freeways and offshore structures. Hereby, rock-socketing offers an attractive solution for achieving maximal tip resistance and improving the load transfer capabilities of the foundation element. In soil profiles with very soft surface soils, rock-socketing often provides the only reliable source of axial and lateral resistance. This thesis investigates the nonlinear performance behavior of piles embedded in soil stratigraphies consisting of soft surface soil underlain by rock via experimental and numerical studies. Model scale test results of a (0.254m) 10in diameter pile, socketed in simulated rock, and subjected to quasi-static, reverse-cyclic lateral loading, provided reference performance data for a series of future experimental studies on large scale rock-socketed piles. Via numerical studies using the FEM tool Abaqus, this thesis complements the experimental research program, by first validating a previously conducted experiment published in literature and using the modeling experience gained from this preliminary exercise by seeking to replicate the test observation numerically. Results obtained from the model simulation provided pile response profiles that agreed reasonably well with experimental observations. Structural failure was observed through plastic hinging about two pile diameters below soil surface and captured well by the numerical model. The numerically obtained load deflection behavior over-predicts the experimental pile stiffness and indicated larger pile capacities compared to experimental observations. A discussion of the experimental results, numerical model development, modeling assumptions, modeling results including important pile demand parameters such as shear and moment demands, as well as recommendations for the upcoming large-scale tests are provided.

CHAPTER 1

INTRODUCTION

1.1 Problem Statement and Objectives

Rock-Socketing deep foundation provides attractive benefits—e.g., substantial reduction of lateral displacements—for carrying lateral loading in addition to its high axial load capacity. Modeling of foundation response to lateral loading constitutes complex soil-rock-structure interaction, dominated by the structural element's flexural rigidity. The $p-y$ method of analysis remains the single most widely used method for design of drilled shafts in rock (Turner 2006). Insufficient supporting case history data, however, inhibit existing design methods from being regarded as having a high reliability level (Guo and Lehane, 2016). To date, a single study by Reese (1997) presents the only extensively published design criteria for selection of $p-y$ curves in rock. Input parameter recommendations are vague and unsubstantiated by broad experience; however, despite these sources of uncertainty, $p-y$ relationships are widely employed (NCHRP, Turner 2006). U.S. DOT funded research efforts (Gabr et al, 2002, Liang et al, 2009) have supplemented test studies, but limitations such as the assumption of linear Moment-*EI* relationships (e.g., Gabr et al, 2002) and inability to obtain reproducible performance predictions among the two test studies pose challenges for selecting suitable resistance formulations beyond their original development. Aside from the limited availability of validated $p-y$ curves for rock, previous research predominantly focused on geotechnical response aspects of rock-socketed piles without considering complex interaction effects inherent to the pile curvature integration and differentiation procedures and their effect on structural response behavior. Impedance contrasts between strong rock layers and soft surface soils yield abrupt changes in pile moment profiles which translate into amplified shear forces at the rock-socket interface, originating from differentiation of the fourth order differential beam equation. The foundation engineering community has experienced much controversy over whether the large resulting shear demands are real, or if amplified shear forces are artifacts of the $p-y$ analysis method. This effect is particularly pronounced in cases where high lateral forces and moments are transferred into the ground over a relatively small distance (e.g., short stubby socket in high-strength rock). Shaft design will be governed by shear, challenging the design engineer to provide adequate

shear resistance without increasing the foundation costs disproportionately or adversely affecting constructability by constricting concrete flow, with consequences of construction damage due to closely spaced transverse rebar. Validation of potential shear amplification (or the lack thereof) with field load tests and verified advanced numerical analysis is missing in existing literature. However, the correct evaluation of shear demands at soil-rock socket interfaces is vital since the shear demand may govern the drilled shaft's structural design.

In preparation of a large-scale testing program on rock-socketed piles at UC Irvine (UCI), geared towards studying the magnitude of shear amplification at the rock-soil boundary of large diameter pile foundations and providing the engineering community with design recommendations regarding rock-socketed pile foundations, a pre-test model-scale experiment was executed in the UCI Structural Laboratory. The objective of the model-scale experiment was to validate the test setup, study the influence of important boundary conditions, assess the instrumentation techniques, and to gain preliminary insight into the small-scale specimen non-linearity. The experimental work will be described in detail by Favaretti (2018). A summary will be provided in Chapter 4.

This thesis accompanies the model-scale experiment through numerical analyses using the software tool Abaqus and seeks to develop a calibrated numerical model that can be used to verify basic performance parameters of the pile-soil system as well as to validate the observed damage evolution and failure mechanism in the pile element. This understanding will be fundamental in assessing the magnitude and distribution of shear stresses within the pile boundary regions of interest and in verifying the placement of the proposed instrumentation for the future large-scale experiment.

1.2 Structural Representation of Tip Fixity

Current literature provides limited amounts of well-documented and sufficiently instrumented experimental research data on rock-socketed piles under lateral loading. Published studies primarily focus on the overall pile behavior as well as the back-calculation of $p - y$ resistance functions for rock and soil strata. Less attention has been directed to the response behavior of foundation systems in soil strata with strong impedance contrasts present at the interface between stiff rock and soft soil and the resulting implication on the structural design of

the foundation system.

With the uncertainty of the rock condition (i.e., strength) in the near soil vicinity due to weathering and drilling, most engineers struggle with selecting an appropriate structural boundary condition to properly represent the pile embedment condition at the pile tip. The depth at which full rotational and frictional resistance can be provided is often estimated; particularly when project budgets do not allow for extensive rock sampling and laboratory testing. Figure 1-1(a) shows a simple, free-head pile embedded in rock. Figures 1-1(b) – (d) display the variety of structural pile tip boundary conditions available to represent the rock socket in an analytical or numerical model. Figure 1-1(b) assumes the case of complete structural fixity (e.g. zero displacement and zero rotation) across the entire rock socket. This assumption creates a strong stiffness contrast at the interface of the two foundation materials. In this case the pile can be treated as a fixed cantilever beam without considering the lateral resistance of the surface soil. Figure 1-1(c) relaxes this assumption by assigning pinned supports that provide a lateral displacement restraint but do not enforce rotational fixity within the rock socket. A more advanced model is displayed in Figure 1-1(d), in which the soil-pile interaction and the rock- pile interaction is represented through a series of non-linear springs (i.e., $p-y$ springs) corresponding to the respective material properties. In this approach the pile is allowed to rotate and displace according to the spring stiffness assigned to the rock socket and the soil material.

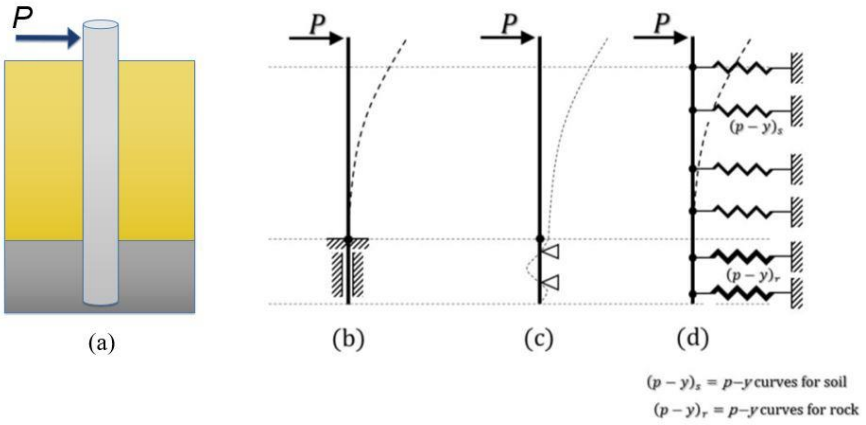

Figure 1-1 Pile soil models - representation of pile embedment

1.3 Modeling Approaches and Inherent Design Challenges

The two most commonly employed analytical tools for the design of laterally loaded, rock-socketed pile foundations are the subgrade reaction method, commonly referred to as 'beam on nonlinear Winkler foundation (BNWF) model, and the 3D continuum approach described by Poulos (1971). While 3D FEM models are computationally more expensive, a properly done 3D FEM model can provide deeper insight into the pile response behavior and better capture the interaction between the structural and soil nonlinearities and the influence of the system's boundary condition. In contrary, BNWF models such as the $p-y$ curve model are extremely easy to use and have been implemented in inexpensive, commercially available software that is user-friendly and provides a reasonable level of accuracy for most foundation studies.

Previous studies, however, have shown that the use of the $p-y$ type analyses on laterally loaded piles embedded in rock yield unexpectedly high values of shear forces, which translate into unreasonably high structural design demands (Turner, 2006). This shear amplification stems from the back-calculation of the shear force profile along the pile shaft through the differentiation of the moment profile following the traditional fourth order differential beam equation. A sharp change within the moment profile translates into a spike within the shear force profile. This effect is particularly pronounced for pile-soil systems with very strong stiffness contrasts and is an immediate by-product of the mathematical BNWF formulation. Consequently, a pile subjected to lateral forces and moments at the pile head, develops shear forces in the vicinity of the rock–soil interface with much larger magnitudes than the applied lateral load at the pile head. The high demands in shear translate into a multitude of intrinsic construction issues such as the need for very dense transverse reinforcement spacing that potentially restricts the concrete flow and lead to the formation of air pockets within the concrete shaft.

Much controversy exists in the geotechnical community whether the large resulting shear demands are real, or if high shear forces are a pure artifact of the analysis method, as explained above. Therefore, the engineering community pursues two different design approaches: (1) some engineers design for the magnified shear forces resulting from the $p-y$ type analyses and provide the increased amount of transverse reinforcement near the rock-soil boundary, (2) others ignore the spike in shear force obtained analytically and design the pile for a shear force equal to

the applied lateral force at the pile head.

Over the past years, national design recommendations such as the Caltrans “Bridge Design Practice” manual published in February 2015, acknowledged this uncertainty [Section 16.4.4 : “When CIDH piles tipped in rock are analyzed for lateral loads, the p-y method reports shear demand forces that exceed the seismic overstrength shear, V_0, calculated demand in the column. The abrupt change to high-stiffness p-y springs may amplify shear force to more than $5V_0$ within the rock socket.”..... “However, there is ongoing debate over whether the design force is "real" and whether the discretization of distributed soil reaction to nodal springs is appropriate at the rock interface.”]. To be conservative, Caltrans recommends the increase of the pile diameter to accommodate the larger interface shear or suggests the provision of additional transverse reinforcement to resist the amplified shear demand. Yet, uncertainty remains, and the engineering and construction communities are in need of clarification through experimental and advanced numerical studies.

1.4 Thesis Structure

The primary objective of this thesis is to (1) provide a review of recent experimental and numerical research studies on laterally-loaded rock-socketed foundation systems, (2) take advantage of state of the art 3D finite element modeling capabilities to numerically replicate a rock-socketed pile specimen which was tested to complete failure in the laboratory, and (3) to gain preliminary insight into the performance behavior of the model-scale test specimen to provide more confident recommendations for the future large scale experimental testing program.

Following this introduction, Chapter 2 of this thesis will provide a comprehensive review of research documented in literature and summarize large scale field testing as well as analytical and numerical studies on rock-socketed foundations. Chapter 3 will describe a numerical validation study using the large-scale field test program by Yang (2006). This exercise is used to familiarize the author with modelling techniques pertaining to laterally loaded piles. Chapter 4 will present the experimental test and describe important performance parameters of the model-scale specimen in the laboratory. Chapter 5 focuses on the development of a calibrated, nonlinear

3D pile soil model of the test specimen. Details of the model formulation, boundary conditions, material relationships and loading protocols will be provided. Preliminary results obtained from Abaqus will be used to perform a side-by side comparison with the experimental record. Chapter 6 will summarize the findings of this work and provide recommendations for the large-scale testing program through lessons learned from this modelling exercise.

CHAPTER 2

LITERATURE REVIEW

2.1 General Review of Common Modelling Approaches

2.1.1 The subgrade reaction method

The subgrade reaction method, as implemented through the $p - y$ curve analysis algorithm, remains the most globally utilized analytical tool to characterize the response of deep foundations. The method offers practical advantages such as the prediction of fully nonlinear lateral load-deflection response, the ability to incorporate multi-layered soil profiles, the integration of nonlinear stiffness (*M-EI*) behavior, and a completed description of structural demand parameters (shear, moment, displacement, and rotation) (Turner, 2006). Its implementation in commonly used design software makes it an attractive and economical tool within the geotechnical community. Yet its principal limitations include the lack of a strong theoretical basis for $p - y$ curves and the limited verification through instrumented load tests (Turner, 2006). Specifically, the interaction of soil or rock between adjacent springs is not considered and the $p - y$ curves are not related directly to any measurable material properties.

The mathematical fundamentals of the subgrade reaction method are derived from the governing differential equation of a beam on an elastic foundation (Hetenyi,1946), as shown in Eq 2-1.

$$EI\ \frac{d^4y}{dz^4} + P_z \frac{d^2y}{dz^2} - p - w = 0 \qquad \text{(Eq.2-1)}$$

in which *EI* is the flexural rigidity of the foundation, *y* is the lateral deflection at a depth *z* along its length, P_z is the axial load on the pile, p is the lateral soil/rock reaction per unit length of foundation and *w* is the distributed load along the length of the shaft (if any).

Via field measurements of internal pile curvatures along the length of the pile element, the shear force profile, soil reaction profile, pile slope and pile displacement profile can be obtained through double derivation, and double integration, respectively as presented in Figure 2-1. The soil reaction to the pile can be expressed by assembling a series of independent non-linear springs, also known as $p - y$ springs, as shown in Figure 2-2 (after Reese, 1997).

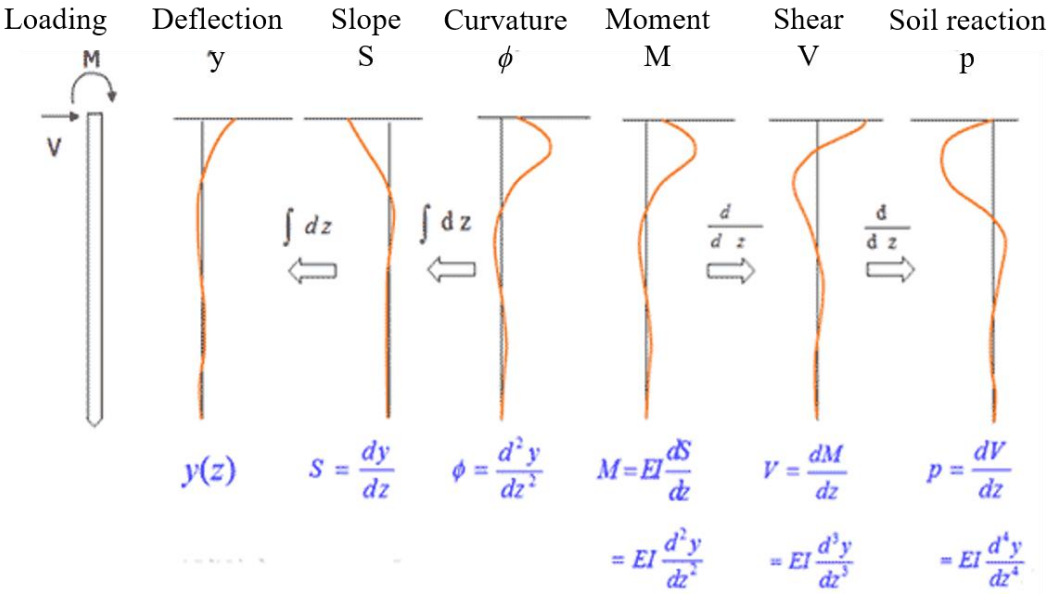

Figure 2-1 $p - y$ derivation procedure from field curvature measurement

(Courtesy: www.FindaPile.com)

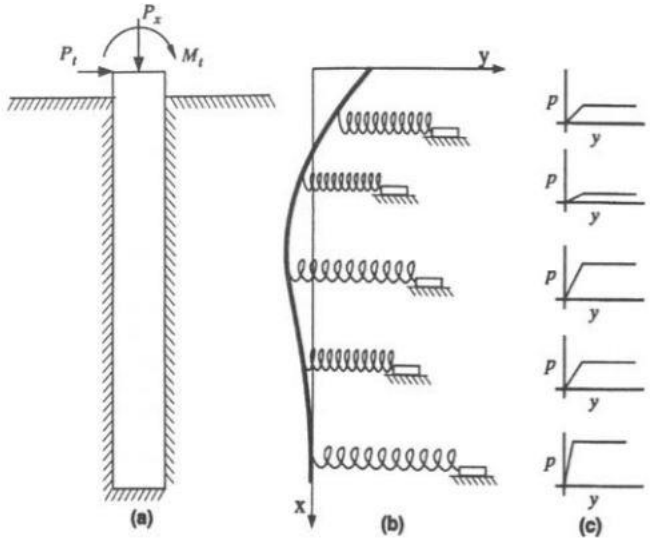

Figure 2-2 Subgrade reaction model based on $p - y$ curve: (a) Elevation view; (b) Elastic line; (c) p-y curves (taken from Reese 1997)

2.1.2 Elastic continuum approach

The elastic continuum approach developed by Poulos & Davis (1980) was based on the boundary element method, in which the pile was modeled as a thin elastic strip and the soil was modeled as a homogenous, isotropic elastic material. This method considers two boundary conditions at the tip of the pile; (1) the pile is completely fixed against displacements and rotations at its base, i.e., near the rock surface, and (2) the pile is free to rotate but fixed against translation (pinned) at its tip. Poulos and Davis (1980) present a series of mathematical relationships for deflections (δ) and rotations (θ) at ground line for free-head piles as shown in Equations Eq. 2-2-a and Eq. 2-2-b.

$$\delta = \frac{P}{N_h L^2}\left(I'_{\delta P} + \frac{e}{L}.I'_{\delta M}\right)/F'_{\delta} \quad \text{(Eq. 2-2-a)}$$

$$\theta = \frac{P}{N_h L^3}\left(I'_{\theta P} + \frac{e}{L}.I'_{\theta M}\right)/F'_{\theta} \quad \text{(Eq. 2-2-b)}$$

$$N_h = \frac{\Delta E_s}{\Delta z} \quad \text{(Eq. 2-3)}$$

where, $I'_{\delta P}$ and $I'_{\delta M}$ are the elastic influence factors for displacements caused by horizontal loading (P) and moment (M), respectively. These factors are applicable to linearly varying soil moduli E_s. Similarly, $I'_{\theta P}$, $I'_{\theta M}$ are the elastic influence factors for rotation. F'_{δ} is the yield displacement factor defined as the ratio of pile displacement in elastic soil to pile displacement in yielding soil for linearly increasing E_s and p_y. p_y in the aforementioned context represents the soil yield strength, which varies from zero at the surface to a value of p_L at the pile tip. F'_{θ} represents the yield rotation factor in a similar manner. e describes the load eccentricity and can be obtained by dividing the pile applied moment (M) by the applied lateral force (P), i.e., $e = M/P$; N_h is the rate of change of the elastic modulus of soil with depth, and L describes the length of the pile.

Randolph (1981) further developed the elastic continuum approach using the finite element method. Although the solutions presented by Randolph cover a wide range of conditions for flexible piles and are presented in convenient closed form solutions, the solutions do not adequately cover the full range of parameters applicable to rock socketed shafts used in practice. Carter and Kulhawy (1992) extended this approach to rigid shafts and shafts of intermediate flexibility which has led to practical analytical tools based on the continuum approach.

2.2 Review of Field Tests on Laterally-Loaded Pile Foundations in Rock

According to Turner (2006), very few lateral load tests on drilled shafts in rock have been performed with the instrumentation necessary to back-calculate resistance functions applicable to rock-socketed pile foundations. Hence a limited amount of $p-y$ relationships for drilled shafts in rock exist. Even though the back-calculation of $p-y$ relationships is not the primary objective of this thesis, a brief review of previous research will allow for better understanding of the research progress on rock-socketed foundations made over the past twenty years. The remainder of this chapter will summarize experimental and numerical studies of laterally loaded, rock-socketed deep foundations in various parts of the United States and abroad.

2.2.1 Frantzen and Stratton (1987)

The first extensively instrumented load tests on rock-socketed piles date back to Frantzen and Stratton in 1987, funded by the Kansas Department of Transportation. The Kansas DOT report titled "P-Y curve data for laterally loaded piles in shale and sandstone" describes the findings of four full-scale lateral load tests conducted in weathered clay shale, sandstone and sandy shale soil conditions. Table 2-1 summarizes the rock quality, type, and strength characteristics at each of the test locations. The test shafts were each 20 cm (8in) in diameter and 4.57m (15ft) in length. The shafts extended 85cm (2.8ft) above the ground line. The load application was performed in two steps: first a three ton (6.6kips) lateral load was repeatedly applied and released to observe cyclic loading effects. Hereafter, loading was monotonically increased to a maximum of 20 tons (44kips) until failure was reached. Loading was terminated when continuous deflection without load increase was observed, in some cases at load levels less than 20 tons. The authors suggested that the rock experienced brittle fracture when the lateral stress against the rock assumed values greater than the shear strength of the rock multiplied by the pile diameter. A conclusive discussion of the failure mechanism during the experimental study was not provided.

Frantzen and Stratton used the subgrade reaction approach as outlined in Reese and Matlock (1956) to back-calculate $p-y$ relationships for each test pile. The authors first determined the pile deflection profiles following the mathematical function shown in equation 2-3, and using inclinometer readings obtained during the experiment:

$$y = A_y \frac{P_t T^3}{EI} + B_y \frac{M_t T^2}{EI} \qquad \text{(Eq.2-3)}$$

where A_y & B_y are deflection coefficients, P_t & M_t are the applied lateral load and moments, and T is the relative stiffness factor, which is defined as $T = \left(EI/k\right)^{0.2}$ with k as the unit modulus of subgrade reaction.

Figure 2-3 presents a generalized bilinear $p - y$ curve for strong, unweathered sandstone and sandy shale. The test data also provided additional information to prove the applicability of stiff clay $p - y$ curves in certain types of weathered shale.

Table 2-1 Test location and rock characteristics reported by Frantzen and Stratton, 1987

Test location	**Unconfined compression strength [tsf]**	**Rock quality designation**	**Color/Type**
Lane Shale	17	71%	grey shale, thin zones of limestone and siltstone
Bonner Springs	0.6	40%	grey and green clay shale
Renner Road	34	55%	shaley sandstone
Leavenworth Road	60	45%	tonganoxie sandstone

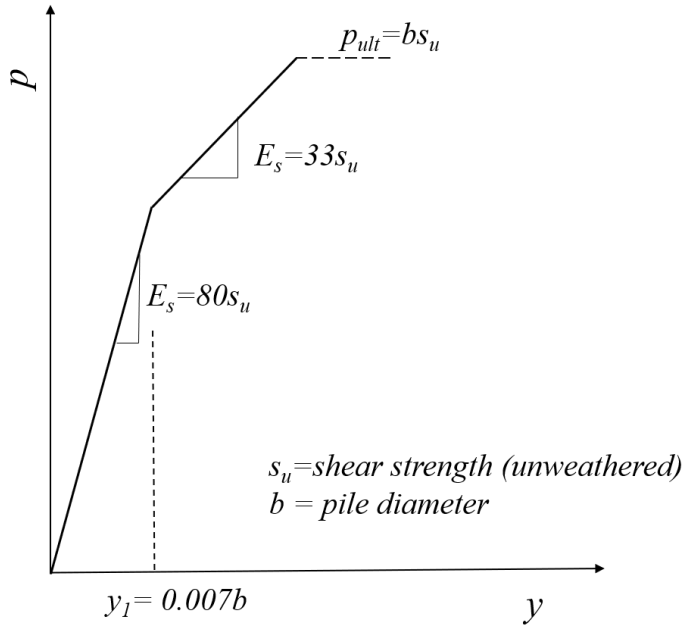

Figure 2-3 Proposed bilinear $p - y$ curves for sandstone & sandy shale (i.e., strong and unweathered rock), (reproduced after Frantzen and Stratton, 1987)

2.2.2 Dykeman and Valsangkar (1996)

Dykeman and Valsangkar (1996) conducted 40g centrifuge testing of eight caissons embedded in a variety of smooth and rough rock socket conditions. The rock was replicated using a mixture of cement, sand, bentonite and water. The prototype dimensions of the caisson correspond to 1.0m (3.3 ft) in diameter and 2.54m (8.3 ft) in length. Dykeman and Valsangkar compare their experimental results with analytical predictions using Carter and Kulhawy (1992) and Poulos and Davis (1980), as well as previous experimental studies by Frantzen and Stratton (1987). Disagreement between all analytical methods, and previous tests and the test observations by Dykeman and Valsangkar was found for all centrifuge experiments. No $p - y$ relationships were derived.

2.2.3 Reese (1997)

In 1997, Reese was the first researcher to propose $p - y$ relationships for weak rock. To date, these relationships remain the most commonly employed lateral resistance functions in commercially available software. Reese (1997) used data from two load tests of rock-socketed piles. The first load test performed under the sponsorship of the Florida Department of Transportation was executed in Islamorada, Florida and consisted of a drilled shaft, with a diameter of 1.2m (47in) and a total length of 15.2m (50ft). The pile was embedded into a brittle, vuggy coral limestone over a depth of 13.3m (43.6ft). A small layer of sand above the rock was retained by a steel casing during construction. Lateral loading was applied at a distance of 3.51m (11.51ft) above the rock surface. The second field study analyzed by Reese (1997) was a lateral load test conducted on a drilled shaft socketed into sandstone at a site near San Francisco. The shaft was 2.25m (7.4ft) in diameter with a rock-embedment length of 13.8m (45.3ft).

In addition to the $p - y$ relationships derived from the experimental results, Reese (1997) provided a general recommendation for the ultimate resistance of weak rocks (q_{ur} < 6.9MPa (1000psi)) based on the limit equilibrium given in Eq. 2-4 & Eq. 2-5 below.

$$p_{ur} = \alpha_r q_{ur} b \left(1 + 1.4\left(\frac{x_r}{b}\right)\right) \qquad 0 \le x_r \le 3b \qquad \text{(Eq.2-4)}$$

$$p_{ur} = 5.2\alpha_r q_{ur} b \qquad x_r \ge 3b \qquad \text{(Eq.2-5)}$$

where, q_{ur} is the compressive strength of rock; α_r is the strength reduction factor (assumed to be 0.33 for RQD of 100 and to increase linearly to unity at RQD of 0); b is the diameter of pile; and x_r describes the depth below rock surface.

Reese correlated the pile with a beam resting on an elastic, homogenous and isotropic solid with an initial modulus of K_i (p_i / y_i) which can be expressed in Eq. 2-6 using symbols of rock.

$$K_{ir} \cong k_{ir} E_{ir} \quad \text{(Eq. 2-6)}$$

where E_{ir} = initial modulus of rock; and k_{ir} = dimensionless constant. The values for k_{ir} are derived from experiments and are shown in Eq. 2-7 & Eq. 2-8.

$$k_{ir} = \left(100 + \frac{400 x_r}{3b}\right); \qquad 0 \le x_r \le 3b \quad \text{(Eq. 2-7)}$$

$$k_{ir} = 500; \qquad x_r \ge 3b \quad \text{(Eq. 2-8)}$$

Following the derivation process described above, Reese (1997) proposed a $p - y$ resistance function as shown in Figure 2-4 (a). This $p - y$ curve consists of three characteristic zones. The initial linear portion of the curve can be described using Eq. 2-9 up to a displacement y_A which corresponds to the deflection at which the initial tangent slope intersects with the $p - y$ curve for rock.

$$p = K_{ir} y \qquad \text{for } y \le y_A \quad \text{(Eq. 2-9)}$$

where K_{ir} = initial slope of the curve, y is the lateral displacement of the pile at the respective depth. The transitional, non-linear portion of the curve is described by a quartic relationship as expressed in Eq. 2-10. Upon reaching the ultimate resistance of the rock, the $p - y$ curve plateaus at a maximum capacity of p_{ur}.

$$p = \frac{p_{ur}}{2}\left(\frac{y}{y_{rm}}\right)^{0.25} \qquad \text{for} \ge y_A \ ; \ p \le p_{ur} \quad \text{(Eq. 2-10)}$$

$$y_{rm} = k_{rm} b \quad \text{(Eq. 2-11)}$$

$$p = p_{ur} \quad \text{(Eq. 2-12)}$$

where, p_{ur} is the rock mass' ultimate resistance, which can be obtained through uniaxial compressive strength testing of the intact rock multiplied by a strength reduction factor (α_r) to account for the depth below the rock surface. The displacement y_{rm} is the transition segment of the $p - y$ relationship based on the shaft diameter b and a constant k_{rm} (Eq. 2-11). k_{rm} is a constant used to establish the overall stiffness of the curve and ranges between 0.00005 and 0.0005. Figure 2-4(a) shows the $p - y$ resistance function for weak rock and an additional function for strong rock is illustrated in Figure 2-4 (b).

Rock is considered to be strong if the unconfined compressive strength q_{ur} is greater than 6.9MPa (1000 psi). Reese recommends performing load testing if the anticipated horizontal deflection exceeds 0.04% of the shaft diameter.

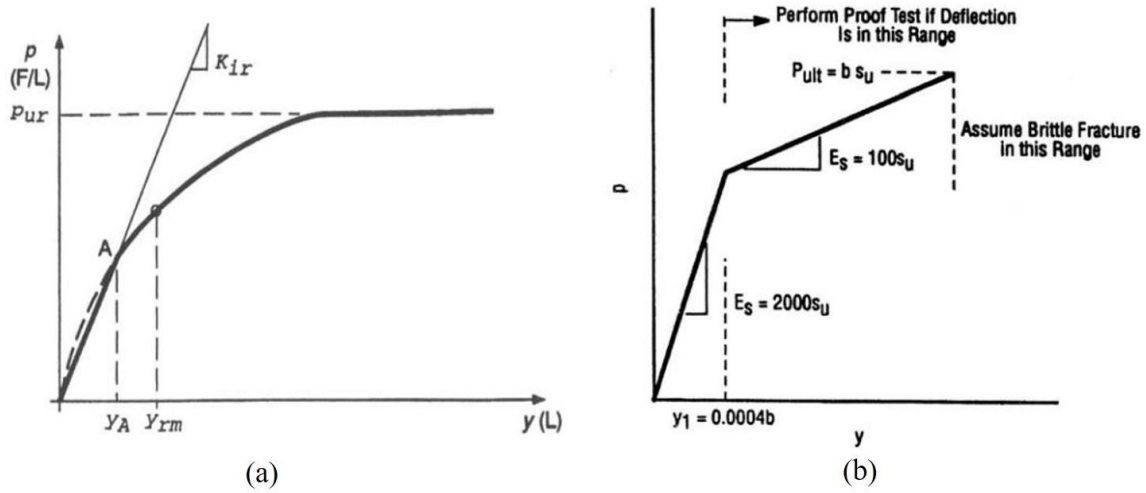

Figure 2-4 (a) Proposed p-y curve for weak rock (Reese 1997) (b) Simplified bilinear curve for rock (taken from Ensoft Inc. 2004)

The $p - y$ relationships for weak and strong rock as presented in Figures 2-4 (a) and (b) have been incorporated into the most widely used computer programs used by state DOTs for analysis of laterally loaded rock-socketed foundations. The Reese research group first developed a software tool published as an academic script under the program name COM624P (Wang and Reese, 1993). Its current commercial version, LPILE (Ensoft Inc., 2004), allows the user to assign a limited number of soil or rock types to each subsurface layer and provides a suite of $p - y$ resistance functions as well as the option for user-defined $p - y$ formulations.

2.2.4 Gabr et al. (2002)

Funded by the North Carolina Department of Transportation, Gabr et al. (2002) conducted lateral load testing of drilled shafts embedded in weathered rock. Two full-scale lateral load tests were performed at three test sites each, located in Nash, Caldwell, and Wilson Counties. The test setup was similar at each site and is depicted in Figure 2-5. Table 2-2 summarizes the basic geometry and rock type at all three test locations. All shafts were 76.2cm (2.5ft) in diameter. Each test location had two shafts, namely a long and a short shaft. Test shafts

were spaced approximately 7.62m (25ft) apart and were constructed with permanent steel casing. In addition to the permanent casing, vertical reinforcement steel was placed in each test shaft to increase flexural strength and allow for the attachment for strain gauges. Lateral loading was applied approximately 0.3m (1ft) above the excavated ground line elevation.

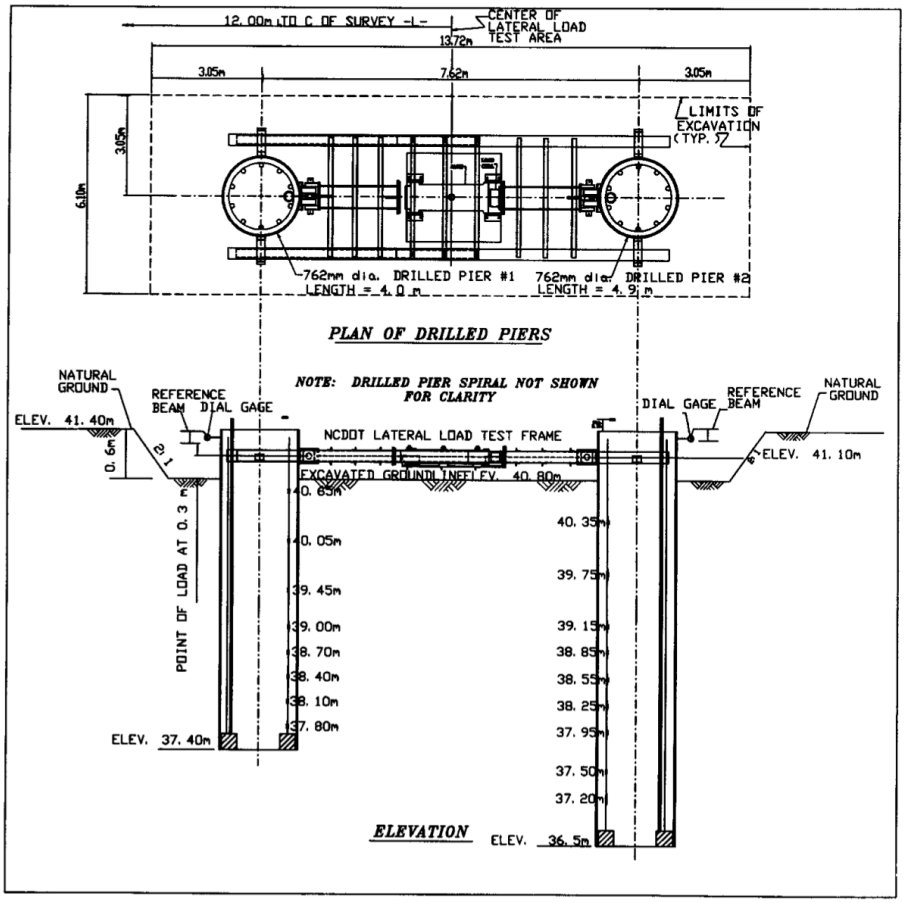

Figure 2-5 Shaft layout for NCDOT testing (Figure taken from Gabr et al., 2002)

The ultimate objective of the Gabr et al. (2002) study was to propose a new $p-y$ model for weathered rock. The combined experimental-numerical research yielded the derivation of a hyperbolic $p-y$ relationship described below. The results of the field tests were then used to validate the procedure for the design and analysis of other laterally loaded drilled shafts embedded in weathered rock profiles. The procedure used to construct the $p-y$ curve formulation according to Gabr et al. (2002) is summarized hereafter.

Table 2-2 Summary of North Carolina field test geometries and results after Gabr et al. (2002)

	Nash County		**Caldwell County**		**Wilson County**	
	Short Shaft	Long Shaft	Short Shaft	Long Shaft	Short Shaft	Long Shaft
Length (m)	3.35	4.57	4	4.8	4.85	5.71
Slenderness ratio	5.19	6.8	7.2	8.27	6.36	7.49
Max. Load (kN)	534	979	1334	1334	1681	1681
Max Shaft-Top Deflection (m)	0.135	0.036	0.089	0.023	0.034	0.055
RQD (%)	< 25	< 25	< 30	< 30	≈ 60	≈ 15
Rock type	Meta-Argillite		Gneiss		Crystalline	

Step 1: Calculation of Coefficient of Subgrade Reaction

Following Vesic (1961), the coefficient of subgrade reaction, n_h, is calculated using the drilled shaft diameter (b), and the rock's Poisson ratio (υ) and Geological Strength Index (GSI), as shown in Eq. 2-13

$$n_h = \frac{0.65E_m}{b(1-\upsilon^2)}\left[\frac{E_m b^4}{E_p I_p}\right]^{\frac{1}{12}} \quad \text{(Eq.2-13)}$$

where E_p is the modulus of elasticity of shaft, I_p is the moment of inertia of shaft.

Step 2: Calculation of Flexibility Factor

A flexibility factor, K_R is computed following Eq. 2-14

$$K_R = \frac{E_p I_p}{E_m L^4} \quad \text{(Eq.2-14)}$$

where, L is the embedment length of the shaft.

Step 3: Calculation of point of rotation.

The turning point (T_0) is defined using Eq. 2-15 as a function of the embedded shaft length.

$$T_0 = (1 + 0.18 \log K_R)L \quad \text{(Eq.2-15)}$$

Step 4: Calculation of I_T number and Subgrade Reaction

$$I_T = -28 - 383\log\left({}^{T_0}/_{L}\right) \quad I_T \geq 1 \qquad \text{(Eq.2-16)}$$

$$k_h = n_h b \qquad (0 \leq z \leq T_0) \qquad \text{(Eq.2-17)}$$

$$k_h = I_T n_h \qquad (T_0 < z \leq L) \qquad \text{(Eq.2-18)}$$

Step 5: Calculation of ultimate resistance of rock mass p_u

The ultimate resistance of rock mass is calculated using the equation proposed by Zhang et al. (2005) which assumes a smooth condition for side shear resistance.

Step 6: Constructing the $p - y$ curve.

The hyperbolic $p - y$ curve is constructed using Eq. 2-19 once all parameters of the subgrade reaction have been calculated.

$$p = \frac{y}{\frac{1}{k_h} + \frac{y}{p_u}} \qquad \text{(Eq.2-19)}$$

2.2.5 Yang (2006)

Yang (2006), Liang et al. (2009) conducted a total of four fully instrumented tests on drilled shafts socketed in rock funded by the Ohio Department of Transportation (ODoT) and the West Virginia Department of Transportation (WVDoT). The tests were executed at two different sites, namely Dayton in Ohio and Pomeroy-Mason, near the Ohio River separating Ohio and West Virginia. The tests were conducted to examine the accuracy of existing $p - y$ methods at the time of the experimental studies and to evaluate the weak rock $p - y$ criterion proposed by Reese (1997).

Test Site 1: Pomeroy - Mason

Two test shafts were constructed at the Pomeroy-Mason site. The test piles were drilled in the Ohio river bedrock. Both shafts had diameters of 2.44m (8ft) in the rock-socketed segments and a diameter of 2.59m (8.5ft) above the bedrock. Both shafts were cased above bedrock using a 25 cm (1.0in) thick steel casing. The total shaft lengths of Shaft #1 and Shaft #2 was 30.9m (101.4ft) and 34.4m (112.9ft), respectively. The rock socket length of both shafts was 12.2m (40ft) and 17.3m (56.8ft), respectively. Shaft #1 extended 10.8m (35.4ft) above the ground and Shaft #2 was 11.4m (37.4ft) above the ground. The rock was overlain by a soil layer

with a thickness of 7.9m (26ft) and 5.7m (18.8ft) at the location of Shaft #1 and Shaft #2, respectively. Figure 2-6 illustrates the test setup for the Pomeroy-Mason specimens.

The drilled shafts were constructed with a concrete of compressive strength of 35.2 MPa (5.1ksi) and internally reinforced with 28 #18 longitudinal rebar (ρ_s = 1.54%) with 10.1cm (4in) cover. The equivalent section modulus of the drilled shafts was 29.3GPa (4250ksi). Lateral loading was applied approximately 10m (33ft) above the soil surface. Lateral loading was applied by tensioning a tendon that was wrapped around the two drilled shafts and pulling the tests shafts towards each other. The maximum load applied was 1223kN (275kips). Each load increment was held until the deflection at the top of shafts was stable. To fully mobilize the rock-shaft interaction and to isolate the overburden soils, a 3.35m (11ft) diameter casing was used to form a gap between the test drilled shaft #2 and the soil above the bedrock. This approach suggests that all lateral forces were resisted by the bedrock during the lateral load test.

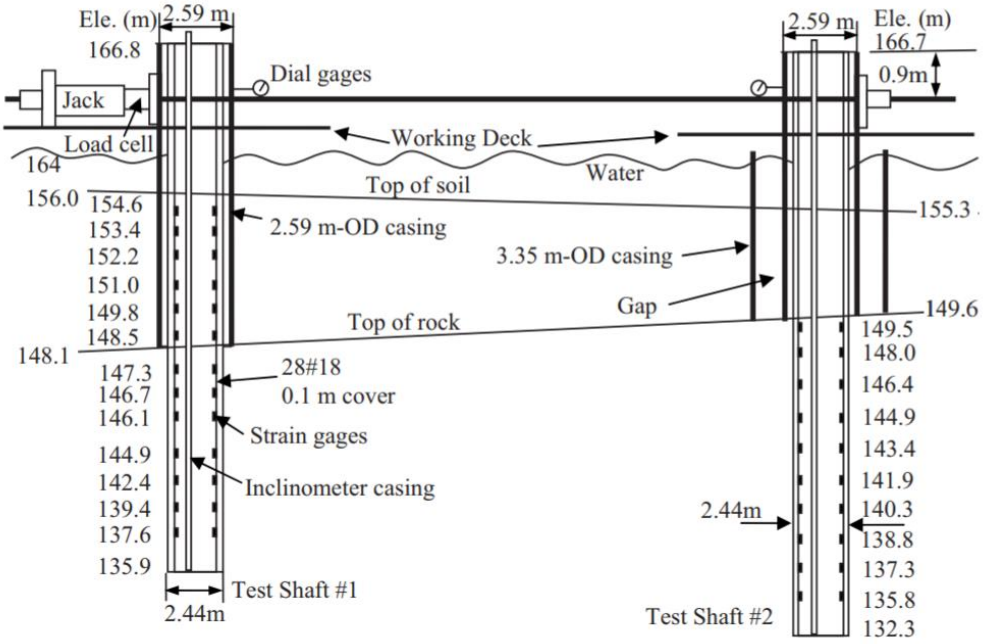

Figure 2-6 Instrumentation and Load test setup at Pomeroy-Mason test (Liang et al. 2009)

Test Site 2: Dayton

Lateral load testing of two 1.83m (6ft) diameter test shafts was performed to assist the design of a new two span reinforced concrete rib arch bridge. The site stratigraphy consisted of fill soils to depths of 1.07m (3.5ft) and 2.44m (8ft), respectively. The fill overlay a layer of grey shale with interbedded limestone, in which the drilled shafts were embedded to a depth of 5.5m

(18ft). The groundwater table was at a depth of 1.8 – 2.4m (6-8ft) below the surface. The shafts were constructed at a center to center distance 5.5m (18ft), and loading was applied by pushing both piles away from each using a hydraulic actuator as shown in Figure 2-7. Both shafts were constructed with a concrete having a compressive strength of 31MPa (4500psi), and reinforcement consisting of 36 #11 longitudinal bars (ρ_s = 1.37%) and #6 transverse spirals.

Loading was applied incrementally up to a maximum load of 5000kN (1126 kips). Each load was held until the rate of deflection at the top of shaft was less than 0.04 inch/min. Figure 2-7 shows the instrumentation and test set up of the site at Dayton.

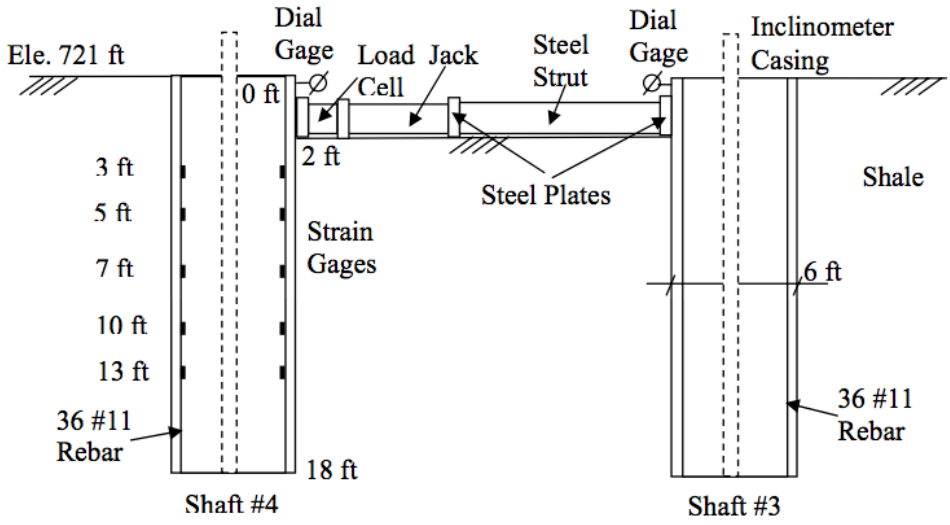

Figure 2-7 Instrumentation and test setup at the Dayton site (Yang, 2006)

Table 2-3 Summary of lateral load tests in Ohio

	Pomeroy-Mason		**Dayton**	
	Shaft #1	Shaft #2	Shaft #3	Shaft #4
Length	31m (101.4ft)	31.3m (112.9ft)	5.48m (18ft)	5.48m (18ft)
Diameter	2.44m (8ft)	2.44m (8ft)	1.83m (6ft)	1.83m (6ft)
Socket Length	12.2m (40ft)	17.3m (56.8ft)	5.48m (18ft)	5.48m (18ft)
Rock Type	Shale and Siltstone		Gray Shale and Limestone	
Modulus of Shaft	29.3GPa (4250ksi)		26.2GPa (3800ksi)	
Max Load	1223kN (275kips)		5008kN (1126kips)	
Max Deflection (at Pile Head)	44mm (1.73in)	94.742mm (3.73in)	2.54mm (0.1in)	3.1mm (0.12in)

The theoretical and numerical analysis results obtained by Yang (2006) were used to develop a hyperbolic $p - y$ criterion. The mathematical expression for the curve is similar to Eq. 2-19 as proposed by Gabr et al. (2002). However, the ultimate resistance of rock per unit shaft length (p_u) is based on three distinct conditions: (i) rock mass failure near surface (based on wedge type failure), (ii) rock mass failure at great depth (based on ultimate shear and normal pressure capacity of rock), and (iii) failure in jointed rock (considers minimum p_u of case (i) and (ii)).

The ultimate resistance of rock mass at great depth is calculated in accordance with Eq.2-20

$$p_u = \left\{\left(\frac{\pi}{4}\right) p_L + \frac{2}{3}\tau_{max} - p_a\right\} D \qquad \text{(Eq.2-20)}$$

where p_L is the normal limit pressure of rock mass which is the major principal stress at failure, p_a is the active horizontal earth pressure based on Rankine's earth pressure theory, and τ_{max} is the side shear resistance based on Kulhawy and Phoon (1993).

Yang (2006) recommends a modification to Reese's expression for the determination of the initial tangent to the $p - y$ curve which considers the relative stiffness between the shaft and the rock, Poisson ratio of the rock and diameter of the shaft (Eq. 2-21)

$$K_i = E_R \left(\frac{D}{D_{ref}}\right) e^{-2\upsilon} \left(\frac{E_p I_p}{E_R D^4}\right)^{0.284} \qquad \text{(Eq.2-21)}$$

where E_R is the elastic modulus of rock mass (based on GSI value of rock (Yang, 2006) and D_{ref} is the reference shaft diameter equal to one foot The proposed $p - y$ hyperbolic curve takes the form

$$p = \frac{y}{\frac{1}{K_i} + \frac{y}{p_u}} \qquad \text{(Eq.2-22)}$$

2.2.6 Parsons et al. (2010)

Parsons et al. (2010) conducted lateral load testing on two shafts with short rock sockets, funded by the Kansas Department of Transportation. Testing under reverse cyclic lateral loading was conducted in Wyandotte County, Kansas. Both shafts had dimensions of 1.06m (42in) in diameter and 2.13m (7ft) in length and were spaced at a distance of 3.65m (12ft) apart from each

other. Both shafts' tips were embedded in weak limestone. The upper soil consisted of 0.5-0.76m (1.5-2.5 ft) of weathered to unweathered sandstone with minimal overburden soil. The average RQD value for the rock mass was considered 70%. The shafts were constructed with 50MPa (7.3ksi) concrete, and reinforced with 12 #11 longitudinal bars (ρ_s = 1.35 %) and #5 bars transverse hoops spaced at 30 cm (12in). Lateral loading was applied 30cm (12in) above the ground level. Pile instrumentation consisted of inclinometers and string pots to record internal and external pile displacements. The results of the test were used to validate LPILE's "weak rock" model and showed that the software could effectively model the lateral load behavior.

The load tests were conducted in three phases. In phase one, loading was incrementally increased until a maximum reverse cyclic lateral capacity of 1780kN (400kips) was reached. Five cycles at each incremental displacement levels were applied to observe potential cyclic degradation. During the second test phase the shafts were incrementally loaded up to 2713kN (610 kips) and 3650kN (820 kips) while applying ten cycles at each load step. During continued loading beyond 3650 kN (820 kips), the loading beams began to yield, and the test terminated to avoid failure in the test equipment. The loading beam was reinforced to enable a third test phase which proceeded to loading the shaft specimens to failure. The corresponding capacity at failure was measured to be 4450kN (1000kips) for both shafts. Inclinometer readings indicated relatively rigid shaft bending behavior during early loading stages with substantial increase of bending at higher loads. A summary of the test parameters and selected results is shown in Table 2-4.

Table 2-4 Summary of shaft tests at Wyandotte County, Kansas

	North Shaft	**South Shaft**
Diameter	1.06m (42in)	1.06m (42in)
Embedment	1.83m (6 ft)	2.13m (7 ft)
Load eccentricity above ground	30cm (12in)	30cm (12in)
Max Deflection at 820kips (10th cycle)[1]	5mm (0.2in)	17.3mm (0.68in)
Nominal Resistance	4448kN (1000kips)	4448kN (1000kips)
Lateral Movement at nominal resistance	11.43mm (0.45in)	24.13mm (0.95in)

[1]Deflection recorded 1.17m (3.86ft) above ground level

The shafts behaved elastically until 1780kN (400kips), i.e., 40% of the ultimate load. Permanent deformations were accumulated for repeated loading starting at 2713kN (610kips) corresponding to 60% of nominal capacity.

The field test data was modeled using LPILE with the objective to identify $p-y$ modelling parameters for limestone (weak rock) within the Reese (1997) weak rock model. The input variables for the model are described in Table 2-5. The overall stiffness of the pile represented by k_{rm} was adjusted within the limiting range proposed by Reese (1997) ($0.00005 < k_{rm} < 0.0005$) and the rock modulus was reduced with respect to the intact rock modulus.

Table 2-5 LPILE Modelling parameters (Parsons et al. 2010)

Shaft Properties		**Rock Properties**		
			Upper layer	Lower layer
Shaft diameter	42 in	Intact Rock Strength (psi)	1750	5068
Shaft length below ground (North Shaft)	6 ft	Intact Rock Modulus (ksi)	370	1040
Shaft length below ground (South Shaft)	7 ft	k_{rm}	0.0005	0.005
Height of load application above ground	12 in			
Concrete strength	7500psi			
Longitudinal Reinforcement	12-#11			
Distance from point of loading to ground surface	12 in			
Yield stress of steel	60000 psi			
Steel Modulus	29,000 ksi			

The computational model developed in LPILE predicted smaller deformations compared to the recorded field data. The predicted nominal resistance was within 10% of field measurements. The authors found the use of the inbuilt "weak rock" model in LPILE to be consistent with the test observations for modelling short rock sockets. They recommend that upper value of 0.0005 must be taken for k_{rm} if no other information is not available. Parsons et al. (2010) also recommend the rock or limestone to be treated as an elastic material (i.e., up to 40% of the nominal resistance) when the number of applied loading cycles is small.

2.2.7 Guo and Lehane (2016)

Guo and Lehane (2016) conducted four instrumented lateral load tests on drilled and grouted shafts in weak calcareous sandstone in Pinjar, Western Australia. The study used cone penetration test (CPT) data for the analysis and design of the lateral response of piles in weak rock and formulated a bi-linear $p - y$ response using q_c (tip resistance) data to estimate the rock's effective strength.

The lateral load test location was situated in a "medium grade limestone". A total of six CPTs and eight Seismic CPTs were conducted within 8m (26.2ft) of the site. The friction ratios varied within 0.4% to 0.6% while the tip resistance, q_c at a depth of three pile diameters was around 35±15 MPa. The SCPT data revealed cemented nature of the deposit with an average shear wave velocity of 950m/s indicating a small strain shear modulus (1.4±0.7GPa). The test specimens, as shown in Figure 2-8, consisted of four piles. Two piles had a diameter of 340mm (13.4in) and two piles had a larger diameter of 450mm (17.7 in). All specimens were 5m (16.4ft) long. The piles were drilled and grouted using a continuous flight auger method. The outer grout was later removed from the exposed sections. Lateral loading was applied 0.9m (3ft) above ground surface. The flexural rigidities of the two pile types after on-site calibration were 7.2MPa (1.04ksi) and 31.75MPa (4.6ksi), respectively.

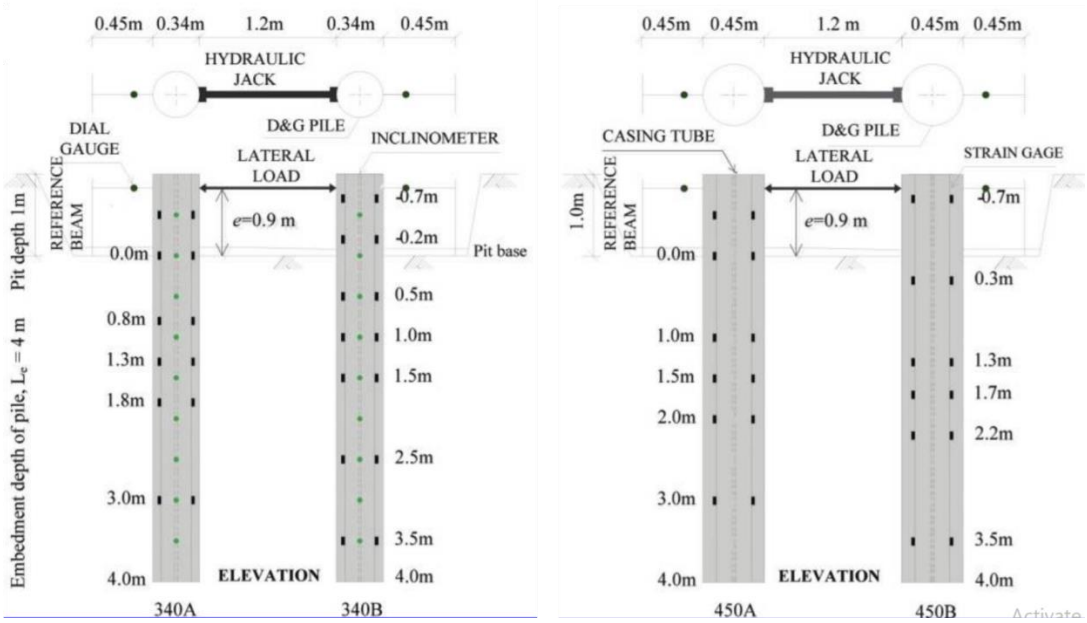

Figure 2-8 Schematic of the test setup configuration at Pinjar, Australia (Guo and Lehane, 2016)

The maximum lateral load applicable to the pile was limited by the lowest capacity of each pile pair. Piles P340B and P450B had lower capacities and failed at lower loads as compared to P340A and P450A. After yielding, the weaker shafts had large continued lateral head deflections. P340B showed deflections of up to 45mm (1.77in) and P450B deflected up to 65mm (2.56in). In turn, the stronger piles P340A and P450A recorded a maximum deflection of only 7mm (0.27in) and 14mm(0.55in), respectively at similar lateral load levels.

Correlation of $p - y$ response with CPT q_c

Guo and Lehane examined a spherical cavity expansion analog for CPT penetration to predict the lateral response of piles in weak rock. The expansion approach to predict q_c described by Yu and Houlsby (1991) has been wide spread and used for sands and clays. Randolph et al. (1994) proposed an expression to relate q_c with the drained spherical cavity expansion limit pressure (p_{lim}) and friction angle (ϕ') in accordance with Eq.2-23.

$$q_c = p_{lim}(1 + \tan\phi' \tan 60°) \qquad \text{(Eq.2-23)}$$

Assuming ϕ' = 40° and a dilation angle of 0°, the q_c values were calculated using p_{lim} values given by Yu and Houlsby (1991). Different combinations of effective cohesion (c') and soil modulus were then deduced which gave q_c resistances of 20MPa (lowerbound), 35MPa (mean) or 50MPa (upperbound) measured at Pinjar. Subsequent analysis of q_c/c' ratio and the ratio of soil modulus with unconfined compression strength (E_s/q_u) in the depth range for the extracted field data presented an ultimate pressure (P_u) of approximately $10c'$ or $2.3q_u$. The study indicated that "if a CPT has been performed at any given weak rock site and if c' and ϕ' can be measured or estimated, the operational equivalent linear elastic modulus (E_s) can be determined using Eq.2-23 and the spherical cavity expansion solution of Yu and Houlsby (1991)". Guo and Lehane suggest a simple bilinear approximation for the rock's $p-y$ characteristic by constructing an initial, elastic slope of $0.8E_s$ extending to a maximum value of p ($=P_uD \approx 0.06q_cD$), the curve getting perfectly plastic at this point. The lateral pile analysis may then be done using readily available commercial software while knowing the pile's flexural rigidity and yield moment capacities.

2.3 Brief Overview of Analytical Studies

2.3.1 Zhang and Einstein (2000)

Zhang et al. (2000) conducted analytical studies to predict the non-linear lateral load-displacement response of rock-socketed shafts by extending the elastic continuum approach. The analysis considered a soil layer overlying a rock layer in which the elastic modulus of the soil and rock varied linearly with depth, while the modulus of rock was assumed to stay constant below the shaft tip. The soil and rock are assumed to behave elastically at small strains and are considered to yield when the soil/rock reaction p (force/length) is greater than the ultimate resistance p_{ult}. Figure 2-9 shows a typical drilled shaft of length L and diameter D embedded within a soil and rock profile. The deformation modulus of the soil was assumed to increase linearly from E_{s1} at the ground surface to E_{s2} at the soil and rock mass interface. The elastic modulus of the rock mass varies linearly from E_{m1} at the soil and rock mass interface to E_{m2} at the shaft tip.

Zhang and Einstein (2000) proposed a simple method that considered local yielding of the rock mass and assumed the rock mass to be elastic-perfectly plastic. A summary of this approach was described as below:

1. Assuming the soil and rock mass are elastic, lateral reaction force (p) is determined after applying lateral load H and moment M.
2. Compare the computed lateral load reaction force (p) with the ultimate resistance p_{ult}, and, if $p > p_{ult}$, determine the yield depth z_y in the soil and/or rock mass.
3. Consider the portion of the shaft in the unyielded ground (soil and/or rock mass) ($z_y \leq z \leq L$) as a new shaft and analyze it by ignoring the effect of the soil and/or rock mass above the level $z = z_y$.
4. Repeat Steps (2) and (3). The iteration is continued until no further yielding of the soil or rock mass occurs.

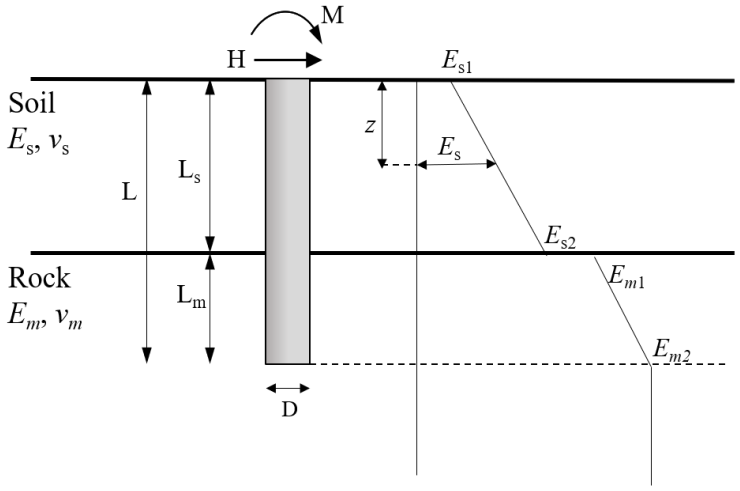

Figure 2-9 Shaft-Soil-Rock System with varying Elastic Modulus

The ultimate resistance of the soil layer is determined for two drainage conditions; undrained or clays ($\phi = 0$) and fully drained or sands ($c = 0$).

For Clay $$p_{ult} = N_p c_u B \quad \text{(Eq.2-24)}$$

For Sand $$p_{ult} = K_p^2 \gamma' z B \quad \text{(Eq.2-25)}$$

$$N_p = 3 + \frac{\gamma'}{c_u} z + \frac{Jz}{B} < 9 \quad \text{(Eq.2-26)}$$

where K_p is the Rankine coefficient for passive earth pressure; c_u is the undrained shear strength of the soil mass; B is the shaft Diameter; γ' is the effective unit weight above soil depth and J is a coefficient ranging from 0.25 to 0.5

The ultimate resistance of rock is determined using Eq.2-27 based on the Hoek and Brown (1988) strength criterion:

$$p_{ult} = (p_L + \tau_{max})B \qquad \text{(Eq.2-27)}$$

wherein τ_{max} represents the maximum shear resistance along the sides of the shaft and p_L is the normal limit resistance determined using correlations to GSI.

2.3.2 Vu (2006)

Vu (2006) provides a comprehensive summary of the analysis techniques on rock-socketed drilled shafts developed based on two primary analysis techniques: the subgrade reaction approach using Reese (1997) and Yang (2006), and the elastic continuum approach based on Carter & Kulhawy (1992), and Zhang et al (2000). The dissertation includes two programming techniques; namely the CRS (Carter Rock Socket) based on Carter & Kulhawy (1992) & ZRS (Zhang Rock Socket) based on Zhang (2000) to analyze 13 full scale tests. The conclusion derived from the work stated that Carter & Kulhawy (1992) and Zhang et. al (2000) methods predicted reasonably accurate deflections for small pile displacements whereas for large deflections the methods suggested by Gabr et al. (2006) and Yang (2006) are more effective. Along with identifying the need to conduct more lateral load tests on rock socketed shafts to very available $p - y$ curve criteria, Vu (2006) proposed the development of new methods for improve our ability to establish a reliable rock mass modulus for rock socket design.

2.4 Finite Element Studies

The analysis of piles in soils using finite difference & finite element models have been largely undertaken in the past but only a few of the models have been validated with experimental results. The design of piles for lateral loading has often been performed using p-y models and the Beam on Non-linear Winkler foundation model. This method does not model the soil as a continuum and hence various field variables are not entirely accounted for. On the contrary, 3D FEM models are computationally more expensive, but when accurately done,

provide more detailed information compared to the BNWF $p-y$ methods. Proper boundary conditions are important to correctly represent the problem.

2.4.1 Brown & Shie (1990)

Brown & Shie (1990) describe a 3D FEM model that included the provision for plastic yield in the soil as well as gapping and slippage at the pile-soil interface. A pile with a diameter of 273mm (10.75in) and a Young's Modulus of 48GPa (7000ksi) was modelled using 27 node brick elements. The base of the pile was fixed against vertical translation, with the center node fixed against displacement fixed in any direction. Two plasticity models were used for the linear elastic soil elements. The first model was a simple, elastic-plastic VM (Von-Mises) model using a constant yield strength envelope which consisted of a uniaxial yield strength of 55kPa (8psi), Young's modulus of 11MPa (1.6ksi) and a poison ratio of 0.45. The second constitutive model used in the analysis was the Drucker-Prager model which was also available in the ABAQUS code at the time. The analysis included results of two types of two soils with different strength parameters; the first with a cohesion of 13.8kPa (2psi) and friction angle (ϕ) of 23° and the second with cohesion 6.9kPa (1psi) and friction angle (ϕ) of 30°. The dilation angle ψ was kept 0° for nonassociated flow.

The pile/soil interface was modelled with 18 node interface elements such that no forces are transmitted upon separation and frictional behavior is induced with coefficient of friction 0.42 upon contact. The results of the computation were compared to those from beam-on-elastic subgrade reaction approach using COM624. A pile-head load vs displacement curve for both the Von-Mises model and the extended Drucker Prager model are shown in Figure 2-11(a) and Figure 2-11(b) respectively.

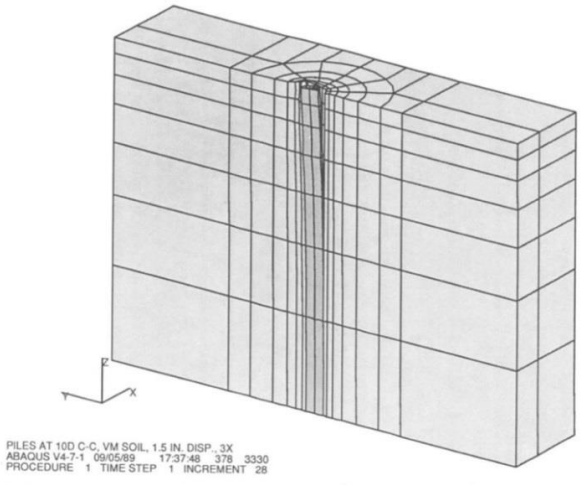

Figure 2-10 View of Three-dimensional mesh with pile displaced laterally, (Brown & Shie, 1990)

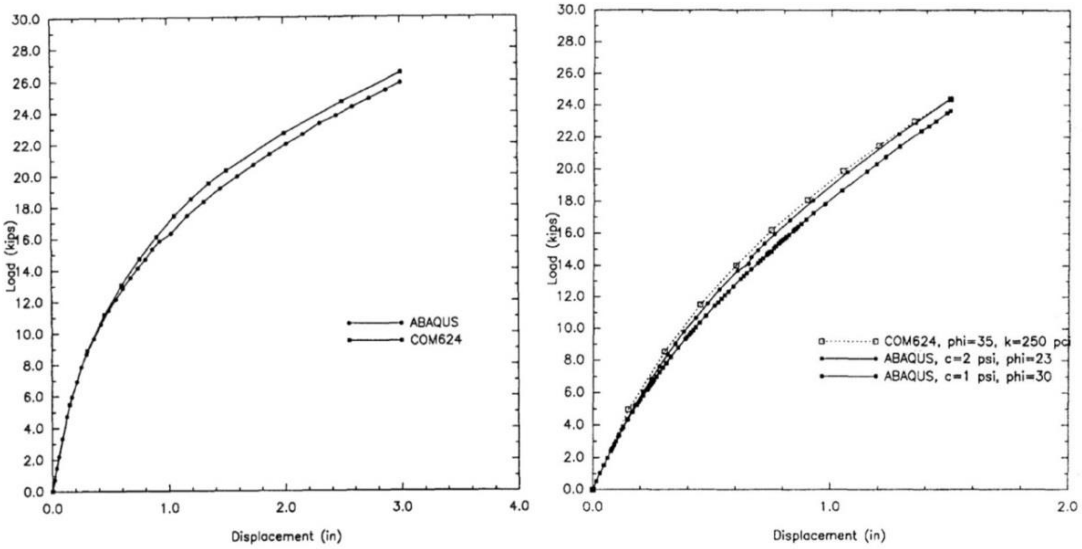

Figure 2-11 Load vs. displacement (a) Von Mises model (b) Extended Drucker-Prager model (Brown & Shie, 1990)

2.4.2 Liang et al. (2009)

Liang et al. (2009) developed a hyperbolic $p-y$ relationship based on the work of Gabr et al. (2002). The analysis used two approaches, namely, the subgrade reaction approach and the elastic continuum approach.

The finite element simulation was used to identify the failure modes of the rock mass under lateral loading, and to establish an empirical relationship for the initial slopes of $p-y$ curves, The shape of the $p-y$ curve is controlled by the initial tangent slope (K_i) and the ultimate resistance of rock mass per unit length (p_u) as per Eq.2-22. Even though Reese (1997)

conducted analytical studies for laterally loaded piles in weak rock, Liang. et al suggest that this approach tended to under-predict the deflections under the applied lateral loads. Hence FEM was used to obtain further insight into the foundation behavior. The model constituted of the drilled shaft consisting of 15-node triangular prism (C3D15) elements and rock mass with C3D8 brick elements. The lateral boundaries around the rock used CIN3D8 infinite elements. The rock constitutive model was the Drucker Prager model. A coefficient of friction of 0.5 was used. The bottom of rock was assumed to be fixed. The study investigated two conditions based on the location of rock failure; a rock mass failure near the ground surface and failure at a great depth. The failure at near ground surface assumes a wedge type failure model while the rock mass failure mechanism in deeper soils accounts for the rock experiencing maximum compressive stresses equal to the rock compressive strength and assumes the rock-shaft side shear strength has been fully mobilized. Yang (2006) provided ultimate rock strength formulations based on these two rock failure criteria. The hyperbolic $p - y$ criterion retains the same mathematical formulation as Gabr et al. (2002)

2.4.3. Yuan et al. (2014)

Yuan et al. (2014) conducted numerical tests to simulate drilled shafts socketed in rock using test data from the Nash and Caldwell County load tests conducted by Gabr et al. (2002). The experimentally obtained load-displacement curves were expanded numerically. Yuan et al.'s work provides a method to predict the ultimate lateral load bearing capacity without taking the rock mass to ultimate failure.

The model consisted of a shaft surrounded by rock extending up to 11 times the shaft diameter and 0.7 times length of shaft below the tip. As described in section 2.2.4, the shafts had a diameter of 0.762m (2.5 ft). A lateral load of 979kN (4355kips) and 1334kN (5933kips) was applied to the Nash & Caldwell simulations respectively. The shaft was modelled as a 3D solid elastic material made up of 15 node triangular prism elements (C3D15). The rock was also simulated using 3D solid C3D8 brick elements. The outer boundary of the rock was simulated using 8-node infinite element (CIN3D8). The Mohr-Coulomb model was adopted for the rock mass.

The results produced a good match with the rock mass mechanics characteristics in the initial elastic stage. The load-displacement curve, as shown in Figure 2-12, was expanded to

higher lateral load. The curve showed initial non-linearity and then becomes linear again indicating that lateral bearing capacity was reached.

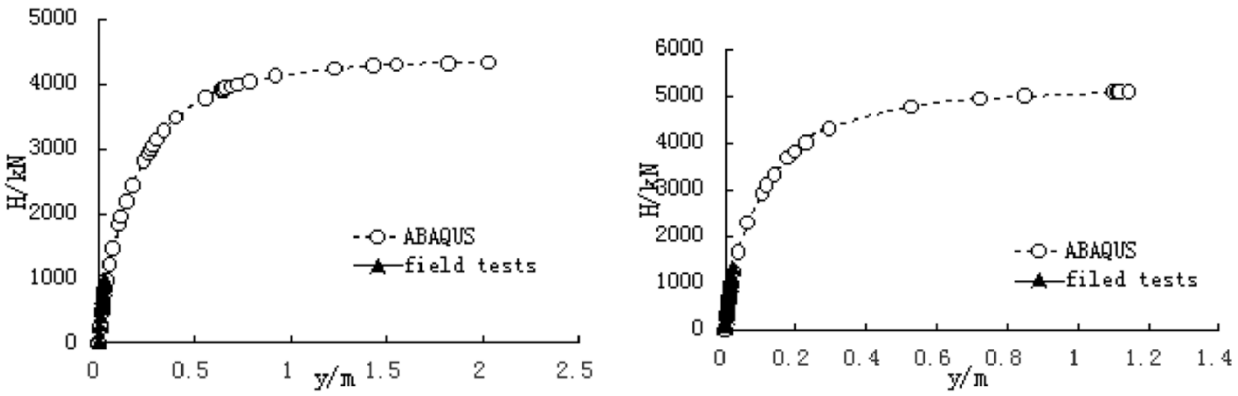

(a) Failure Curve of shaft at Nash (b) Failure Curve of shaft at Caldwell

Figure 2-12 Failure curves for shafts in North Carolina and Numerical tests (Yuan et al. 2014)

Yuan et al. (2014) then compared methods of determining ultimate lateral bearing capacity using the expanded load-displacement curves from the field tests at Nash and Caldwell and the ABAQUS simulation. The methods analyzed were the L1-L2 method (Trochianis et al. 1988) and the hyperbolic function method (Gabr et al. 2002). The results of the L1-L2 method were closer to the actual field tests. This method was then suggested as a preferred method to determine the ultimate lateral bearing capacity. Although the method uses relatively simple parameters, the rock mass is assumed to be homogenous despite large amounts of joints.

2.4.4 Arduino et al. (2014)

Arduino et al. (2014) conducted a numerical study on the behavior of rock-socketed pile foundations with a specific focus on shear magnification at the rock-socket interface. This research effort was funded by PEER (Pacific Earthquake Engineering Research) and the final research report was made available through personal communication and is not officially published yet. The authors compared structural shear demands in rock-socketed drilled shafts using the $p-y$ method and 3D computational models. $P-y$ analyses were executed using LPILE^{TM} (2010) and 3D modeling was conducted using the open-source finite element frame work OpenSees (http://opensees.berkeley.edu) developed by PEER. Arduino et al. used a variety of specimen geometries and rock embedment depths to parametrically evaluate the impact of a

wide variety of geometric and material properties. The research team observed larger shear demands by using the $p - y$ method of analysis.

The 3D models used two separate constitutive models for the rock; a J2 Plasticity model based on Reese (1997) $p - y$ curves and a Drucker Prager Plasticity model. The report concluded that the shear force ratio (shear at top of the pile to max shear force along the pile depth) are largely dependent on the type of constitutive models used for rock analyses and the type of analysis technique (3D or BNWF) with the 3D models holding greater effect on the magnification of shear forces.

2.4.5 Other FEM Studies

In more recent studies, Abdel-Mohti and Khodair (2014) developed two finite element models to study pile-soil interaction under lateral loading. One FE model was developed using ABAQUS while the other numerical model was developed in SAP2000. An HP14X89 A992 steel section with an elasticity of 200GPa (29000ksi) and a yield strength of 345MPa (50 ksi) was embedded in a single layer of stiff clay. The pile had a length of 26.82m (88ft). The base of the rock was fixed attempting to simulate rock embedment of 6.7m (22ft). The Mohr-Coulomb plasticity model was used to model the soil. A varying modulus of elasticity along the soil depth was assumed. Both elements, i.e., the pile and soil, were modelled using eight-node elements (C3D8R). The pile head was laterally displaced by 2cm (0.8in) and no rotation was allowed at the pile head. The pile was loaded under monotonic displacement increments up to specimen failure. This model was not correlated to any experimental studies and purely served the purpose of numerical comparisons among various software platforms. The Abaqus results were compared to results obtained from SAP2000 and LPILE. Abdel-Mohti and Khodair propose that LPILE is feasible for design purposes and a satisfactory agreement between the results of LPILE and the other two relatively complex computational tools was achieved.

CHAPTER 3

NUMERICAL MODELLING EXERCISE

The ABAQUS software package has been widely used to study soil-structure interaction problems and analyze the behavior of deep foundations under various loading conditions. The focus of this study, is to use the software tool for the analysis of laterally loaded piles in soil layers with strong impedance contrasts. Current published studies on laterally loaded piles (static and dynamically loaded) using ABAQUS focus on either a simple, single soil strata or layered strati with small variations of soil stiffness with depth. Large scale tests conducted in Dayton, OH, and reported by Ke Yang (2006) have shown a considerable variation in rock stiffness across the length of the pile. Thus, the FEM study reported by Yang (2006) is used as a basis for modelling the complexity of the system. The modelling exercise was helpful to capture the effects of pile behavior in static soil conditions. It was also useful to understand the important boundary conditions, interactions and constraint restrictions necessary in pile analyses for lateral loading. Although the results presented by Yang (2006) were for a limited deflection level, the exercise provided a useful basis to model a more complicated, cyclically loaded pile with larger deflections.

3.1 Brief Overview of the Numerical Model Developed by Yang et al. (2006)

The Yang et al. (2006) finite element model was developed to replicate the large-scale test described in section 2.2.5 and consisted of two primary components, the drilled shaft and the surrounding rock. Figure 3-1 shows a schematic view of the model with geometry and element assignment as published by Yang (2006). The dimensions and material features assigned to each component are summarized in Table 3-1. The shaft was modelled using C3D15, 15-node triangular elements whereas the rock-mass was modelled using C3D8 brick elements.

The outer boundaries of the rock mass were modelled using 8-node infinite elements CIN3D8 to consider far-field soil effects. This model employed the modified Drucker-Prager constitutive model (CAP model) for the rocks available as a built in constitutive model in ABAQUS and is intended to model cohesive geological materials. The reinforced concrete shaft was modelled as a linear elastic solid with equivalent elastic modulus.

The interaction between the drilled shaft and rock-mass was modelled as a surface-based contact. A frictional interaction using a coefficient of friction, following the linear Coulomb friction theory is used in the tangential direction. The lateral loads were applied step by step after the gravity weight of the shaft-rock system was activated.

The exercise model developed by the author uses a similar modelling protocol as described by Yang (2006). Section 3.2 describes the interactions and boundary conditions used for the exercise in further detail.

Table 3-1 Part and Material Parameters for Dayton test site (Yang, 2006)

Part	**Dimensions**	**Features**	**Material Properties**	
Shaft	18ft. X 6ft. dia (5.48m X 1.83m dia)	Pile Extension above rock=2ft	Density	0.0887pci
		Top embedment=5ft	Elasticity	3800ksi
		Bottom embedment=11ft.	Poisson Ratio	0.15
Top Rock	Depth= 7ft (2.13m)	Elastic Properties	Density	0.034pci
			Elasticity	241ksi
			Poisson Ratio	0.3
		Drucker-Prager Plasticity	Friction Angle	38°
			Dilation Angle	3°
			Cohesion	440psi
			Abs. Strain	0
Bottom Rock	Depth=11ft (3.35m)	Elastic Properties	Density	0.034pci
			Elasticity	590ksi
			Poisson Ratio	0.3
		Drucker-Prager Plasticity	Friction Angle	47°
			Dilation Angle	3°
			Cohesion	819psi
			Abs. Strain	0

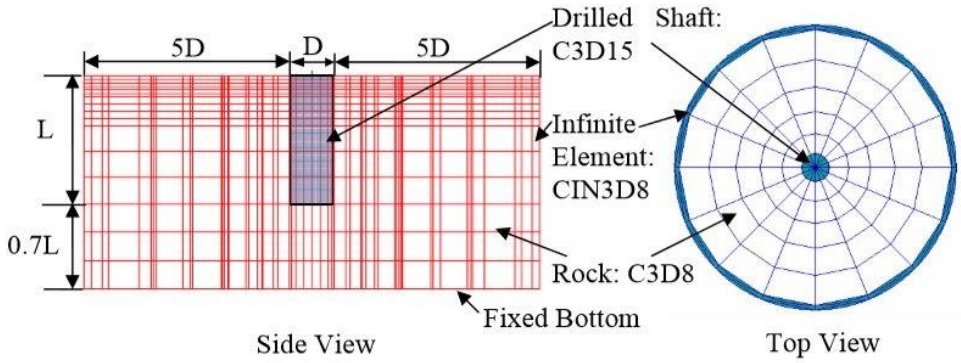

Figure 3-1 Schematic diagram of FEM model for Dayton Test validation, Yang (2006)

3.2 Exercise ABAQUS Model

3.2.1 Geometry and Material Properties

The input material parameters of the practice FEM model developed in this thesis are in accordance with the model created by Yang (2006). The metric system was adopted for ease of physical visualization. The shaft was modeled as a cylindrical solid element. The rock mass extended five times the pile diameter (D) in radial direction and 0.8D below the shaft tip. An elastic-perfectly plastic model with the Mohr-Coulomb failure criterion was utilized to represent the behavior of rock. The inter relation between the Drucker-Prager cohesion (d) and friction angle (β) with the Mohr-Coulomb cohesion (c) and friction angle (ϕ) is given in Eq.3-1 & Eq.3-2. Linear elastic behavior was assumed for the concrete material in the drilled shaft.

$$d = \frac{2c\cos\phi}{1-\sin\phi} \quad \text{(Eq.3-1)}$$

$$\beta = \tan^{-1}\left(\frac{6\sin\phi}{3-\sin\phi}\right) \quad \text{(Eq.3-2)}$$

Table 3-2 summarizes the components of the model with dimensions and material properties in the SI unit system.

The Mohr-Coulomb constitutive model is appropriate when all principal stresses are compressive stresses. The plastic behavior can be modelled using the Mohr-Coulomb failure surface. Figure 3-2 shows the general mathematical formulation of the Mohr's circle. The yield line (failure envelope) of the material is the common tangent to all circles. The failure criterion is linearly related to the shear and direct stresses and takes the form

$$\tau = c + \sigma.tan\ \varphi \qquad \text{(Eq.3-3)}$$

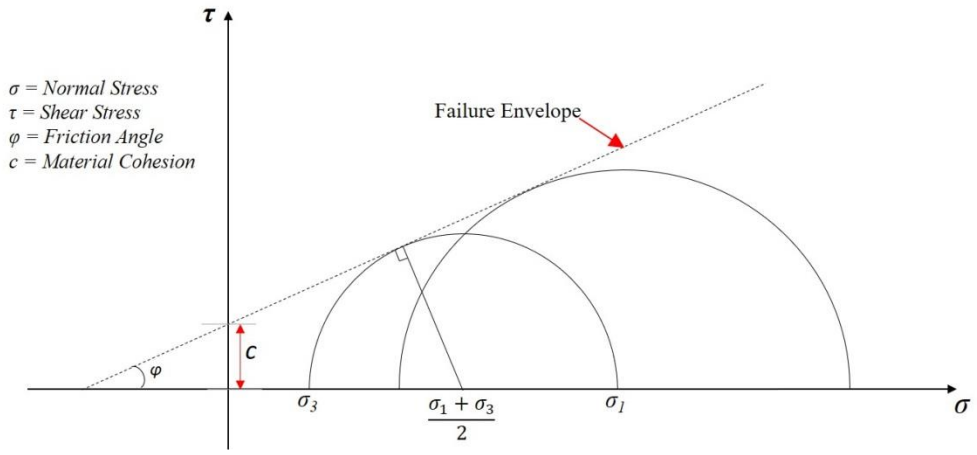

Figure 3-2 Mohr's Circle with linear failure envelope

Table 3-2 Part & Material description for Assessment study

Part	Dimensions	Features	Material Properties	
Shaft	5.5m X 1.8m dia.	Pile Extension above rock=0.5m	Density	2483 kg/m^3
		Top embedment=1.5m	Elasticity	26.2 GPa
		Bottom embedment=3.5m	Poisson Ratio	0.15
Top Rock	20m X 20m 1.5m thick	Elastic Properties	Density	940 kg/m^3
			Elasticity	1.66 GPa
			Poisson Ratio	0.3
		Mohr-Coulomb Plasticity	Friction Angle	20°
			Dilation Angle	3°
			Cohesion	1.06MPa
			Abs. Strain	0
Bottom Rock	20m X 20m 5.5m thick	Elastic Properties	Density	940 kg/m^3
			Elasticity	4.07 GPa
			Poisson Ratio	0.3
		Mohr-Coulomb Plasticity	Friction Angle	27°
			Dilation Angle	3°
			Cohesion	1.73MPa
			Abs. Strain	0

3.2.2 Boundary conditions, Interactions & Loads

To better capture the behavior of the rock material, a geostatic stress condition was first defined prior to applying lateral loading. This geostatic analysis step consisted of the activation of the gravity load within the rock by defining a vertical stress profile that replicates the distribution of effective overburden stresses across the length of the pile foundation. This step is critical in the development of geotechnical models in ABAQUS and may offer an improvement to the original validation model by Yang (2006), where this step is not described.

The following boundary conditions were applied to the exercise model. Displacements were fixed in the horizontal directions along the sides of the rock (U1, U2 = 0) and in all three directions along the base of the rock (horizontal *X* & *Y* as well as vertical *Z* i.e. U1, U2, U3 = 0).

The correct definition of interaction between the concrete shaft and the surrounding soil (i.e., the contact behavior) is an important step when developing the model. The interacting surfaces, i.e., the outer face of the pile and the adjoining rock surface can both be considered planar surfaces in the element domain. This interface may have considerable relative motion. Thus, a surface-to-surface discretization method is used to achieve better accuracies. The concrete shaft has two primary interaction definitions. The interaction is facilitated through the definition of a tangential behavior to simulate friction between the shaft and the rock. As suggested by Yang (2006), the coefficient of friction is defined as 0.5, and allowed for finite sliding to include the effects of nonlinearity. The second interaction mechanism is implemented by defining a "Hard" contact between the pile and the rock and a separation after contact is allowed. The "Hard" contact is a pressure-overclosure definition which states that all contact pressure is transferred between surfaces if they are in contact and there is no pressure transfer if the surfaces do not touch each other. Since the shaft concrete is stiffer than the rock it is embedded in, its surface is treated as the master surface while the rock surface is treated as the slave surface.

The static lateral load was applied at the pile head by a concentrated force on a single node above the head. This node was tied to the pile head using a rigid body constraint. The load was linearly increased over the time step up till the specified maximum load. For the higher load case i.e. 5000kN (1126kips), the rate of loading was faster than the smaller load case i.e. 3130kN (705kips) as illustrated in Figure 3-3 which shows the loading protocol.

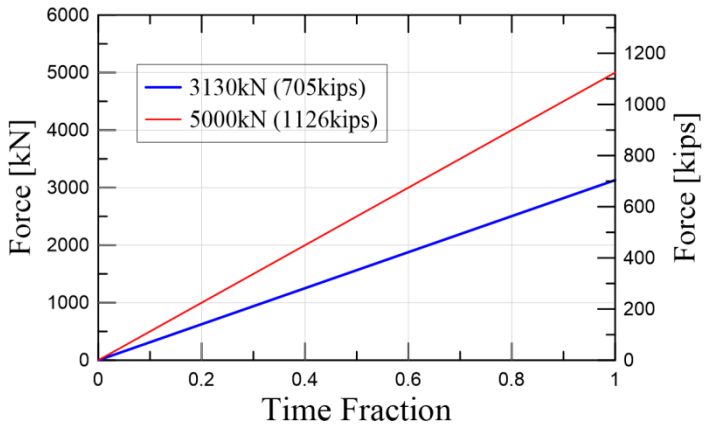

Figure 3-3 ABAQUS load protocol for exercise model

3.2.3 Mesh

The rock surrounding the shaft was large enough to ensure complete stress dissipation. Both, the rock and the pile were modelled using 3D tetrahedral (C3D10) elements as shown Figure 3-4. A total of 6049 & 12785 elements were used for the pile mesh and the rock mesh, respectively. All elements were C3D10 tetrahedral elements as illustrated in Figure 3-4(c). The element size of the rock mesh was increased radially outward, starting from 0.35m (13.8in) around the pile surface to 1.8m (6ft) near the model boundaries. This simplification increased the efficiency of the computation. The mesh size of the shaft was fixed to 0.25m (9.8in) as shown in Figure 3-4(b).

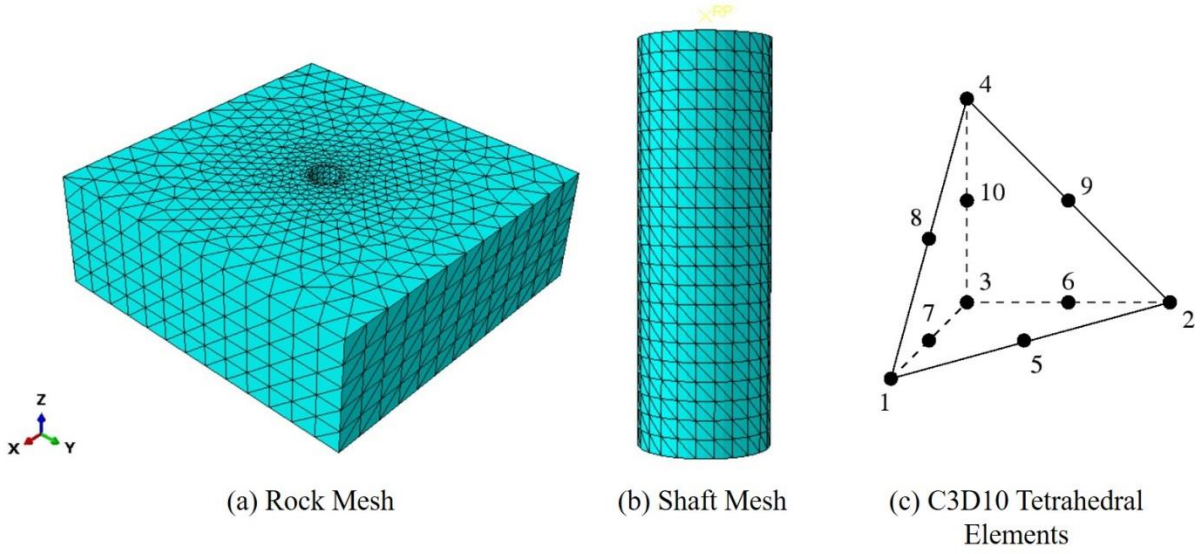

(a) Rock Mesh (b) Shaft Mesh (c) C3D10 Tetrahedral Elements

Figure 3-4 Part meshes & element type for exercise model

3.3 Comparison of results

The vertical and lateral geostatic earth pressure variance along the depth of the rock were compared with analytical calculations to verify the proper distribution of in-situ stresses along the specimen. Eq. 3-4 and Eq. 3-5 describe the analyses of the vertical and lateral stresses.

$$q_z = \Sigma\, \gamma . z \qquad \text{(Eq.3-4)}$$

$$q_{lateral} = K \,.\, q_z \qquad \text{(Eq.3-5)}$$

$$K = (1-\upsilon)/(1+\upsilon) \qquad \text{(Eq.3-6)}$$

where q_z is the vertical overburden pressure as a function of pile depth (z) and rock unit weight (γ) taken as 9221.4N/m^3 (0.034pci) $q_{lateral}$ is the lateral earth pressure, K is the lateral earth pressure coefficient based on soil Poisson ratio (υ) taken in accordance with Eq. 3-6. Figure 3-5 shows the active earth pressure distribution along the depth (z) of the soil mass. S11 denotes the lateral stresses along the X direction in N/m^2.

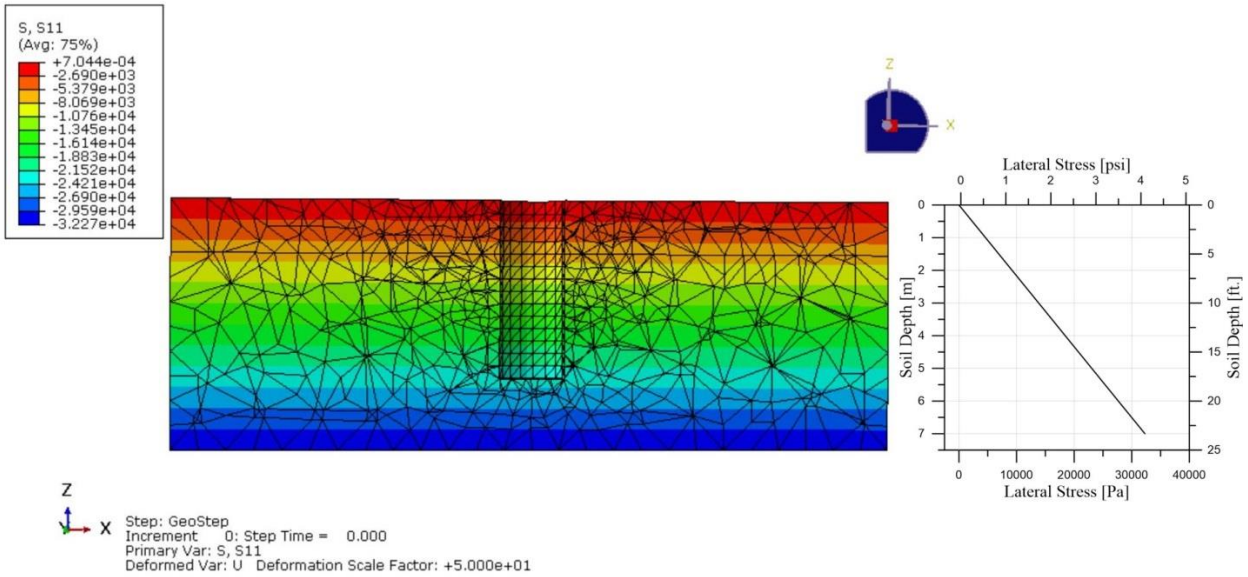

Figure 3-5 Soil Section View: Initial Lateral stress before application of lateral load

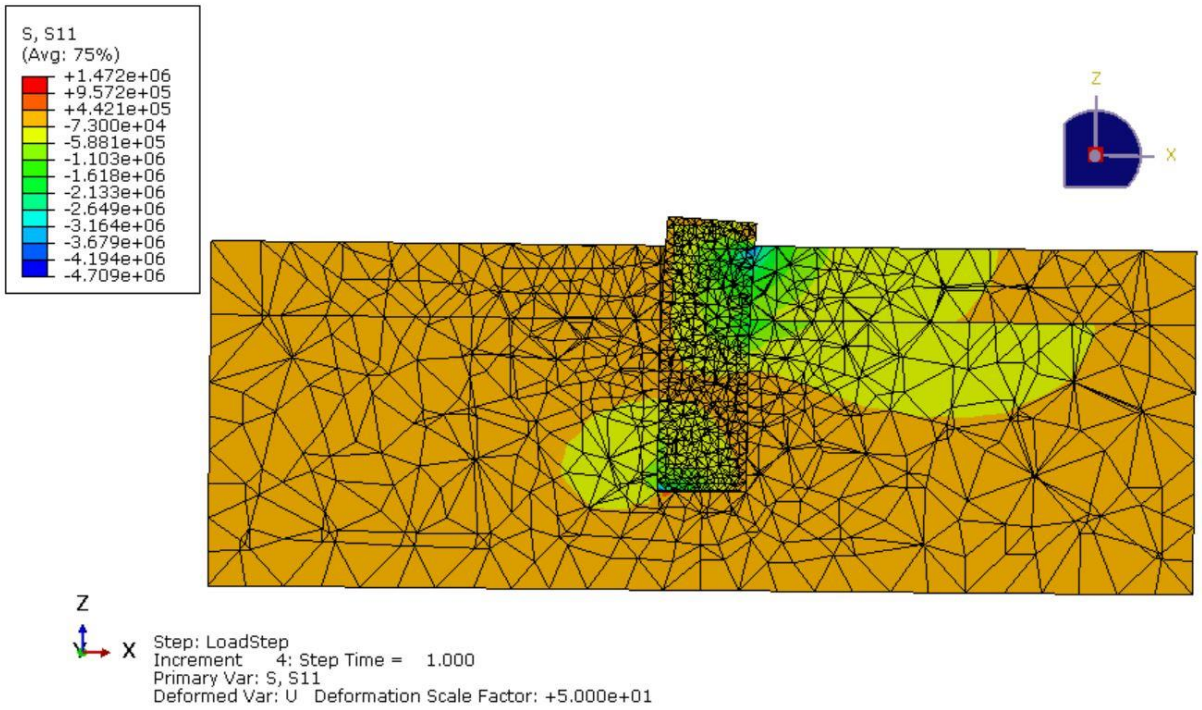

Figure 3-6 Section view: Final lateral stress distribution at end of lateral loading

Figure 3-6 presents a section view of the pile at the stage when 100% of the lateral load has been applied (5000kN). It shows the stress propagation through the surrounding rock. The stress

component S11 represents the horizontal stresses in the X direction in N/m^2. Deformations are scaled to a factor of 50. The width to which the rock extends away from the pile was found to be sufficient to allow for the dissipation of lateral stresses in the loading direction. Figure 3-6 also shows the lateral stresses developed at the pile tip due to potential rotation of the pile within the rock.

Figure 3-7 compares the load-displacement curve obtained from this ABAQUS modelling exercise with the experimental and numerical results obtained by Yang (2006). The model of this thesis shows a good agreement with the test data. In the case of 3130kN of lateral loading, the test pile exhibited a maximum deflection of 1.8mm (0.07in) while the model analysis showed a pile head deflection of 2.1mm (0.08in) (16% error). Similarly, at a lateral load level of 5000kN loaded test pile showed a maximum deflection of 3.1mm (0.12in) while the model head deflection was computed as 3.4mm (0.13in) (9.7% error).

It can also be observed that the results from the exercise model produced a better fit to the field test data than the numerical model developed by Yang. This could be potentially associated with the inclusion of an initial geostatic state of stress in the rock mass prior to applying lateral loading, which was not explicitly described in Yang's validation study. The comparison also shows rotational movement in the pile tip for the exercise model justifying the fact that no rotational constraints were assigned to the pile base. However, a small degree of rotational locking is seen in Yang's analytical results suggesting a fixed tip condition.

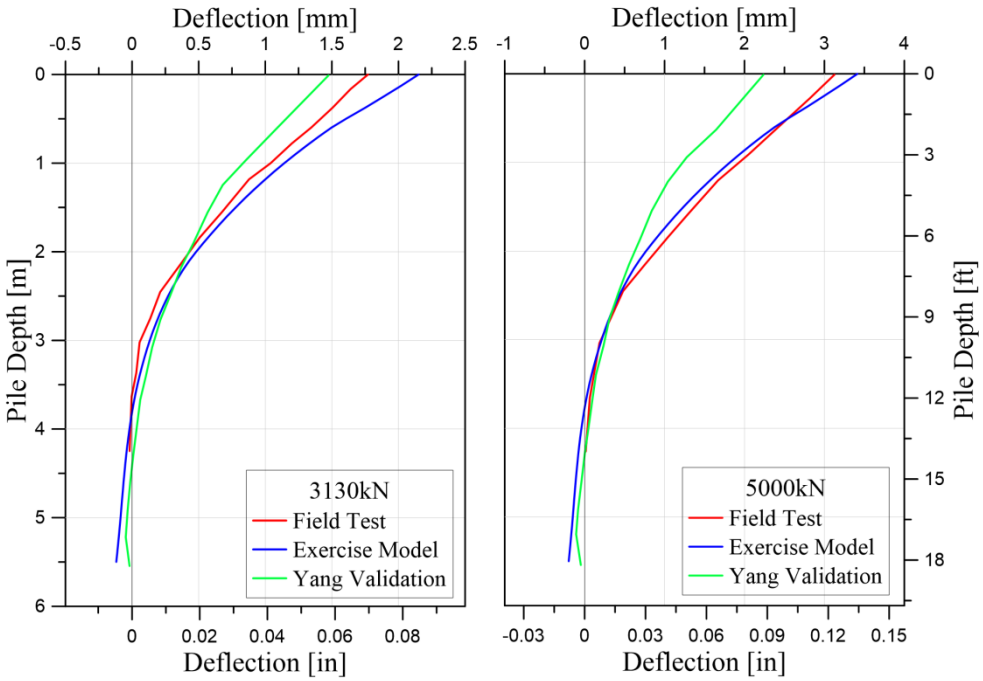

Figure 3-7 Pile Deflection profile for field test and ABAQUS models developed by Yang (2006) and in this study for lateral load levels of 3130kN and 5000kN

In closing, this modelling exercise was helpful in establishing a basic understanding of a laterally loaded pile via. FEM. Although the results present a good agreement with physical tests, the exercise presented data for very small deflection levels (less than 0.17% of pile diameter). With the availability of such small displacements only, it is difficult to extrapolate a prediction of the ultimate behavior under larger and more realistic lateral movements. Since the shaft was modelled as a linear elastic material, non-linear effects are not captured and are difficult to predict in a confident manner.

CHAPTER 4

SUMMARY OF EXPERIMENTAL STUDY

The model scale experiment was conducted in November of 2017 at the UC Irvine Structural Laboratory and is described in further detail in Favaretti, 2018. The model scale experiment was part of a 4-test series on reinforced concrete pile specimens with various boundary conditions and tip fixities embedded in loose sand. The following sections will describe the test setup, geometries, instrumentation, material properties and results of the rock-socketed pile pertaining to this study.

4.1 Test Specimen and Test Setup

The model pile, as shown in Figure 4-1, was installed in a laminar soil box, which consisted of nineteen laminar aluminum frames with a height of 10.16cm (4in). The inner dimensions of the laminar soil box were 99 cm (39in) in width, 185cm (73in) in length, and 219cm (86in) in height. The laminar frames were restrained prior and during testing through a combination of wooden braces and steel sections connected to the laboratory's strong wall. Figure 4-1 & Figure 4-2 present the elevation and plan view of the test specimen. The bottom of the laminar box was filled with concrete to represent the rock material. This concrete consisted of a commercially available grade concrete with a design strength of 27.5MPa (4ksi). The concrete strength of the rock socket is lower than the concrete strength of the pile; this scenario would represent the case of a strong pile in a weak or weathered rock (Typical uniaxial compressive strength of 8MPa - 25MPa). The simulated rock layer had a thickness of 1.016m (42in). The upper soil layer consisted of industrial sand #16, a poorly graded, washed sand. The sand was dry pluviated in place and relative density measurements were taken during pluviation. The soil layer had a total thickness of 1.35m (53 in).

The pile had a total length of 3.18m (125in) length and a diameter of 25.4cm (10in). The pile extended 81.3 cm (32in) outside the upper sand layer. The longitudinal reinforcement consisted of three #3bars and four #4 bars (A_s = 658mm^2). The longitudinal reinforcement ratio (A_s/A_g) was 1.3%. The transverse reinforcement consisted of #4 stirrups spaced at 15cm (6in) along the length of the pile. The transverse steel volume ratio was 1.9%. The concrete cover was 3.8 cm (1.5in) to the outside of the transverse reinforcement.

Per ACI 318-11 Section 21.12, the minimum steel ratio for transverse reinforcement is $0.12f_c'/f_{yt}$ (1.6% for 8ksi concrete and 60ksi steel i.e. #4 at 7in spacing). This reinforcement ratio provides sufficient resistance in shear and bending up to a max lateral applied load of 173.5kN (39kips).

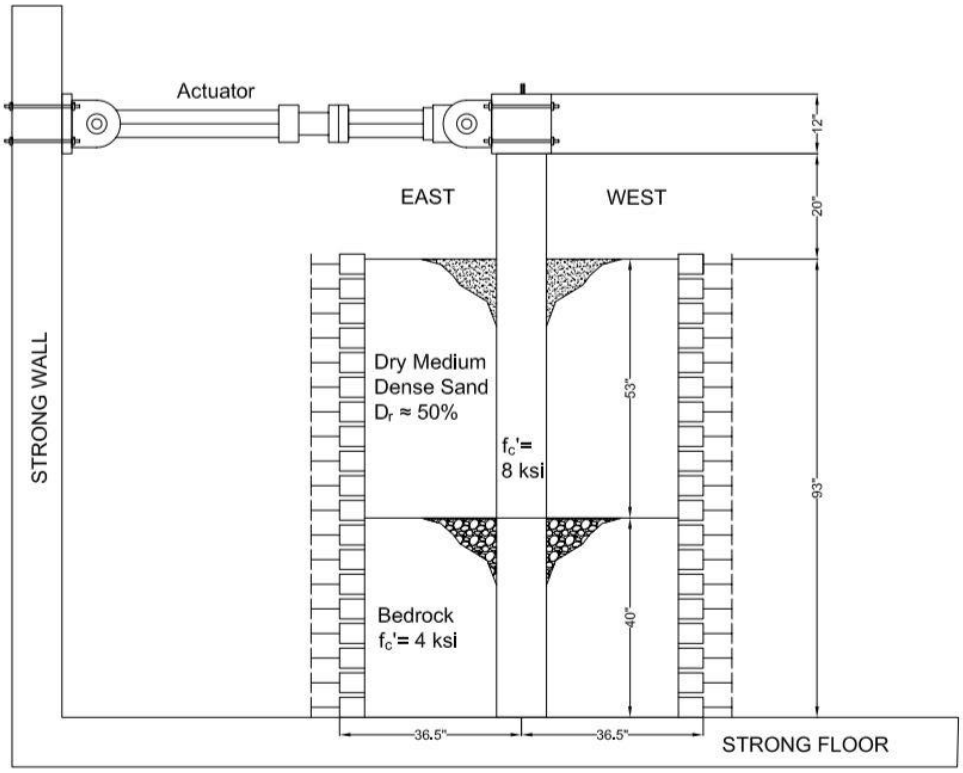

Figure 4-1 Experiment Setup for model scale test (Elevation View)

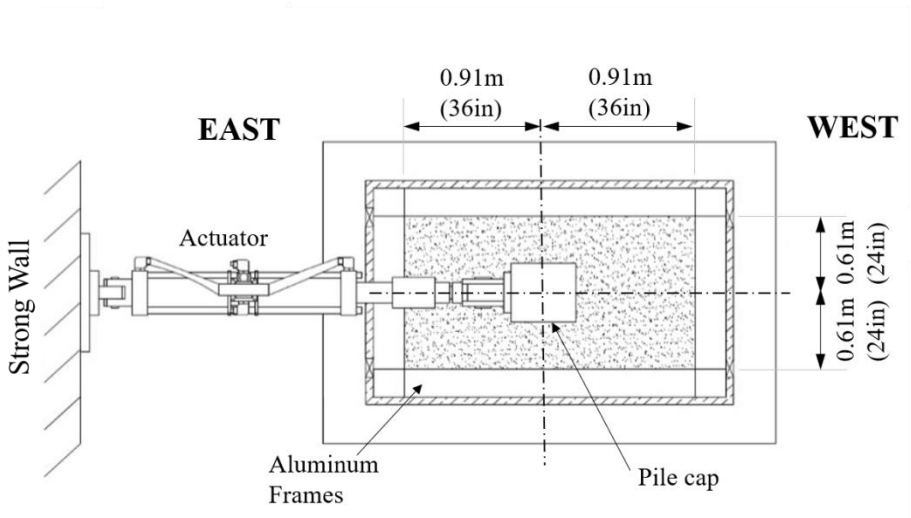

Figure 4-2 Experiment setup for model scale test (Plan View)

4.2 Material Properties

The pile material consisted of polymer concrete with a compressive strength of 55MPa (8ksi). Splitting tensile testing of the material provided a tensile strength of 3.6MPa (550psi). Compressive strength testing of the rock socket concrete showed an average strength f_c' of 27.5MPa (4ksi). No tensile testing was performed for the rock concrete.

The pile's longitudinal and transverse reinforcement steel consisted of nominal A706 Grade60 steel with coupon tests provided by the supplier indicating an yield strength of 60ksi.

The #16 SP industrial grade sand layer had an average relative density of 50%. This density was consistently reached with less than 5 percent deviation during the pluviation process of the material. Density testing was performed using modified proctor molds with known weight-volume relationships placed at various elevations in the laminar soil container. The max dry unit weight of the material was pre-determined through modified proctor testing and found to be 1920kg/m^3 (120lbs/ft^3) at an optimum water content of 8.3%. Direct shear testing suggested a friction angle of the material as 43° and an average cohesion of 5kPa (0.7 psi).

4.3 Instrumentation

The test specimen was heavily instrumented using internal and external sensors. Internal instrumentation consisted of 22 strain gauges attached to the longitudinal rebar at the front and back of the pile in the loading direction. An additional 156 strain gauges were installed on copper tetrahedra to explore a potentially new concept of instrumentation for internal shear stresses. Two sets of external strain gauges were installed in rosette configuration at the shear sides of the pile (i.e. North and South) and located close to the rock socket interface. Two additional external, longitudinal strain gauges were placed at various heights along the pile in bending direction. The west side of the laminar soil box was furnished with soil pressure sensors, spaced at 30cm (12in) in vertical direction. String potentiometers were used to measure the lateral pile displacement outside the soil material. One sensor was placed on the pile cap, in alignment with the hydraulic actuator, and another sensor was placed near the soil surface. Figure 4-3 shows the instrumentation plan of the specimen.

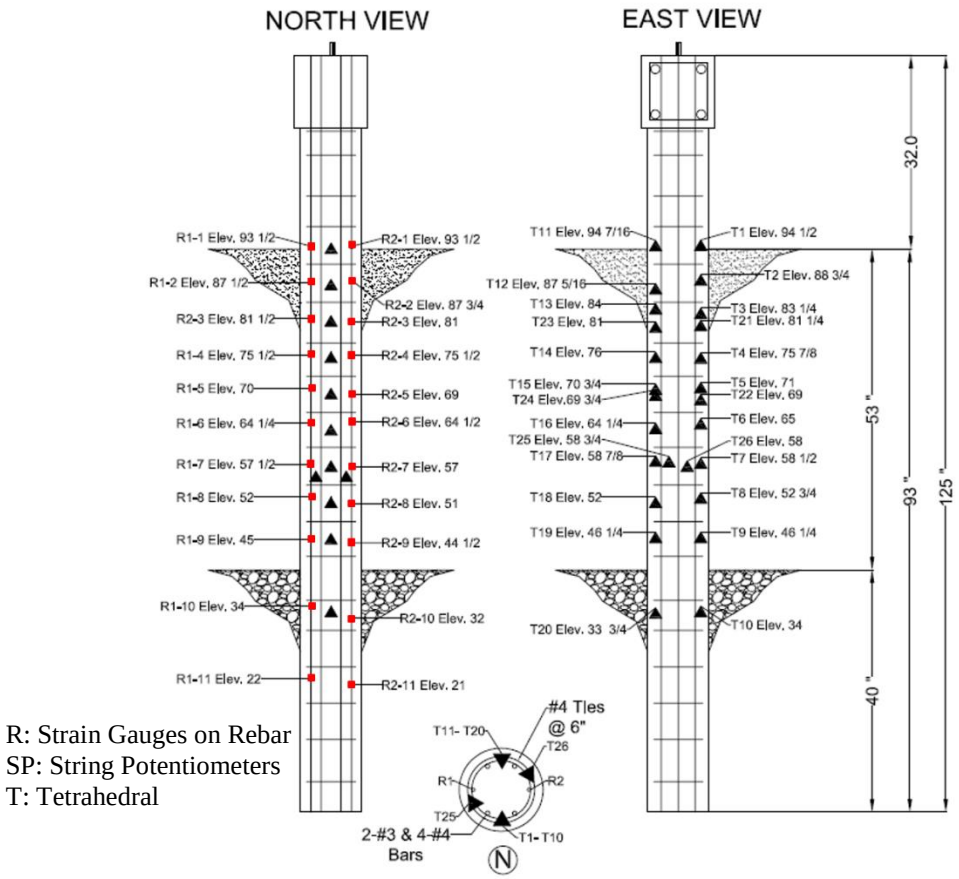

Figure 4-3 Instrumentation plan of test specimen

4.4 Load Application

The pile specimen was subjected to quasi-static reverse cyclic loading up to complete structural failure. The load was applied using a 150 kips hydraulic actuator with a total stroke of 34 inches. Pre-test analytical studies conducted with the computer software LPILE were used to develop a guidance protocol for the lateral load application. In accordance with ASCE 41-06 S1, three load cycles per displacement level were applied up to ultimate capacity, hereafter, cycling was reduced to two cycles per deformation level. The pile was loaded cyclically in East-West direction and the test was performed under displacement control. Preliminary yield displacements levels were obtained using the LPILE software based on which the loading protocol for the test was determined (Table 4-1). The pile head load was recorded across 9176 seconds (~2.5 hours) of testing time. For simplicity, Figure 4-4 shows the time history reference axis as fraction of time.

Table 4-1 Displacement Levels for the test specimen (δy=0.75in.)

δ_y Multiplier	Displacement		Cycles
	in	mm	
1/8	0.1	2.54	3
1/4	0.2	5.08	3
2/5	0.3	7.62	3
1/2	0.4	10.16	3
3/4	0.6	15.24	3
1	0.8	20.32	3
1 1/4	0.9	22.86	1
1 1/3	1	25.4	3
1 1/2	1.25	31.75	3
2	1.5	38.1	3
2 1/3	1.75	44.45	1
2 2/3	2	50.8	3
3 1/3	2.5	63.5	3
4	3	76.2	3
4 2/3	3.5	88.9	3
5 1/3	4	101.6	3
6	4.5	114.3	1
6 2/3	5	127	2
7 1/3	5.5	139.7	2
8	6	152.4	1
8 2/3	6.5	165.1	3
9 1/3	7	177.8	2
10	7.5	190.5	2

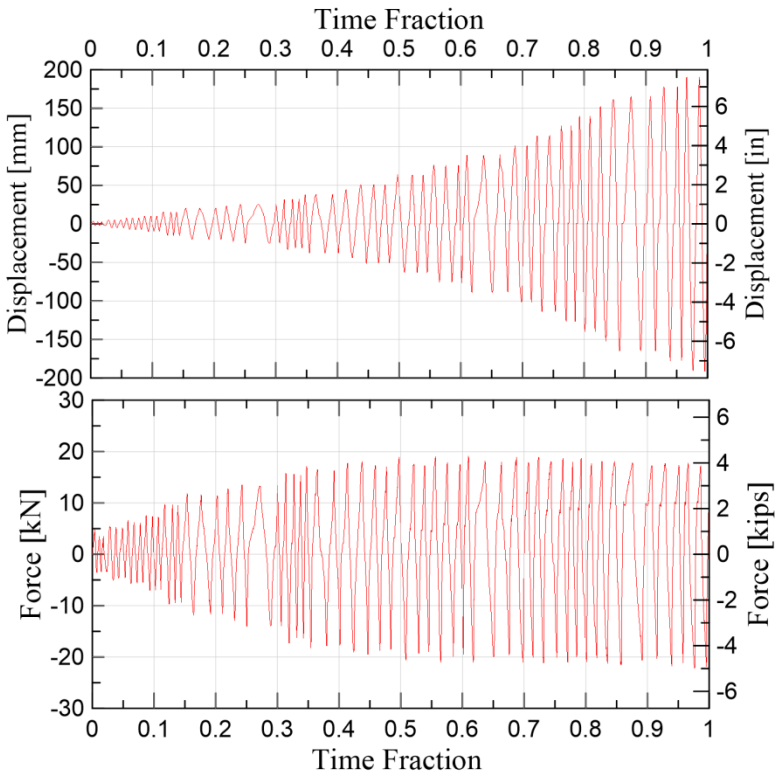

Figure 4-4 (a)Displacement and (b)Force Time history (normalized time)

4.5 Test Results

The specimen was tested on November 21st, 2017. The measured cyclic load time history of the pile is shown in Figure 4-4(b) and the backbone load vs. deflection curves are shown in Figure 4-5. The yield force in push direction was 16kN (3.6kips) at a horizontal displacement of 33mm (1.3in). In the pull direction the yield force measured 17.34kN at a displacement of 33mm. The maximum load observed in the push loading direction was 18.7kN (4.2kips) at 190.5mm (7.5in) of pile head displacement. Post yielding, the pile produced continuous lateral deflection at no further increase of load (approx. 20.5kN).

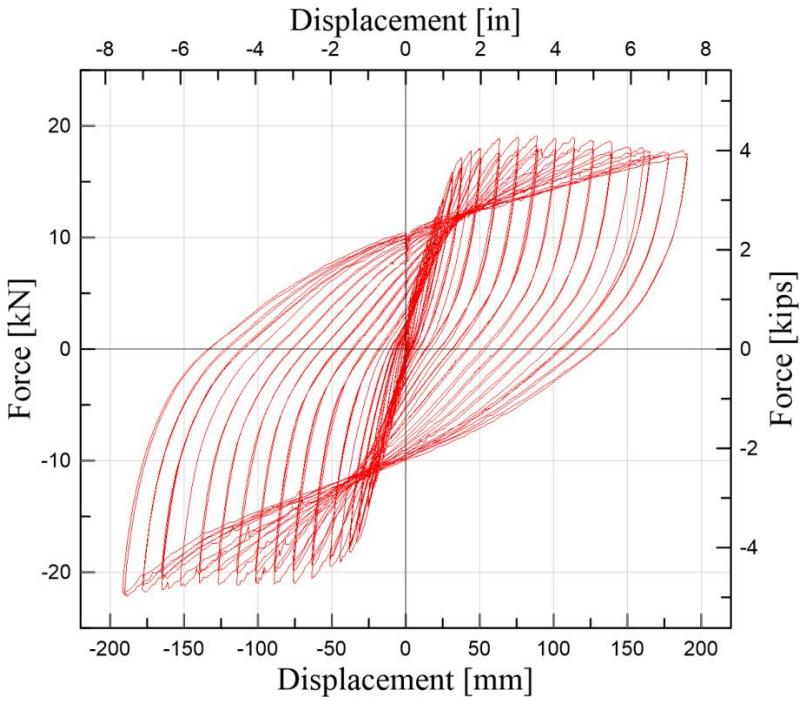

Figure 4-5 Cyclic response of test pile

Observations

In order to visually grasp the displacements on the sand surface layer, a grid marking was created before the application of lateral load. During the test procedure, large movements in the topmost sand layer were evident and the sand tended to cave in towards the pile. This resulted in the top 10-12cm (from initial sand surface) of pile being completely exposed and receiving little to no resistance from the sand. The arching of the sand can clearly be seen in Figure 4-6.

Large horizontal and vertical cracks formed around the pile at different elevations. The most significant cracks developed on the east-west sides (bending direction) of the pile, but they also propagated on the shear sides, causing superficial material detachments. The largest crack (avg. width = 4in) was in the region where the plastic hinge was formed (See Figure 4-7); approximately 72cm (28in) above the top of the bedrock (approx. 2.6 pile diameters below the sand surface layer). Some cracks were visible up to 1.2 pile diameters above the bedrock.

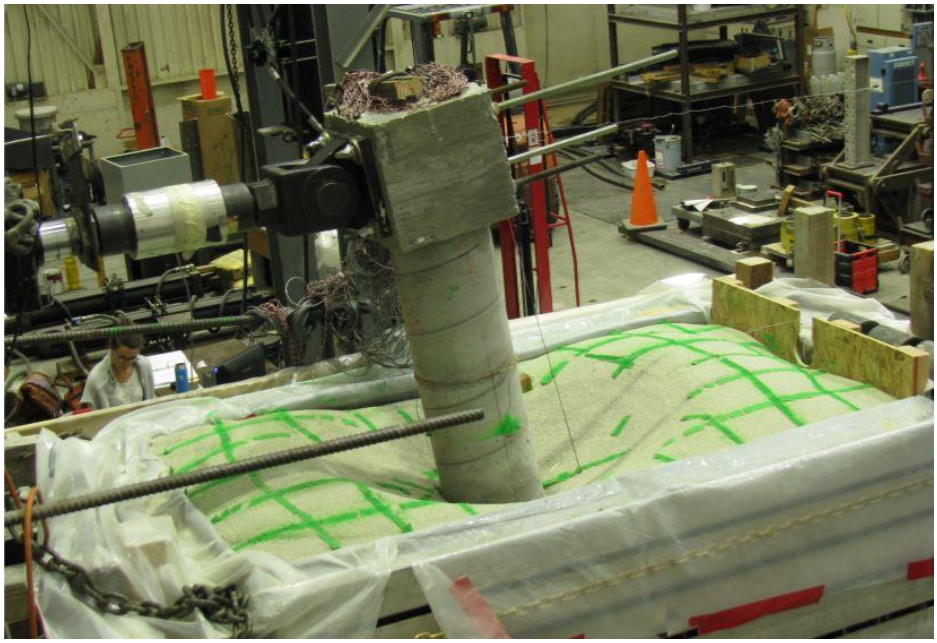

Figure 4-6 Maximum Pile head deflection and sand surface displacement

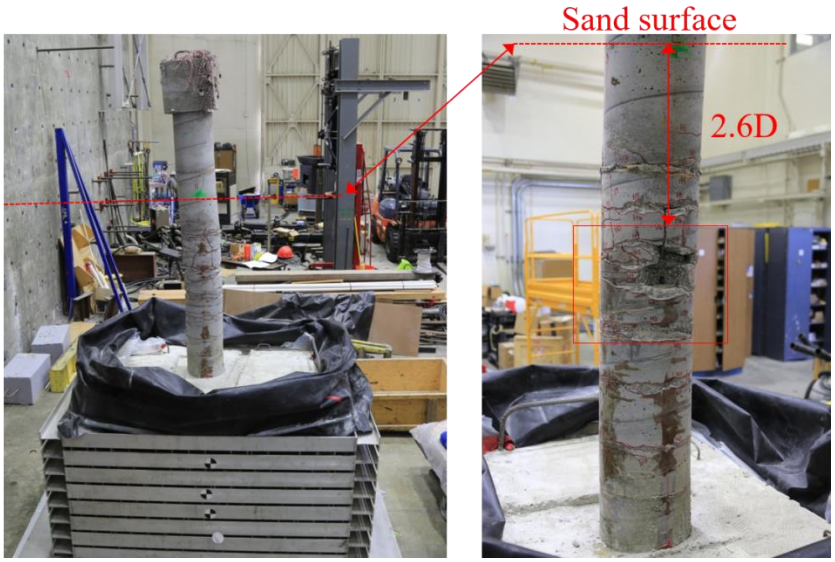

Figure 4-7 Prominent Crack and Plastic Hinge location in Test pile

An important observation was that after removing the overlaying sand layer, the pile did not appear to have displaced at the rock elevation. Subsequently, no cracks or gaps were seen on the surface of the rock (Figure 4-8).

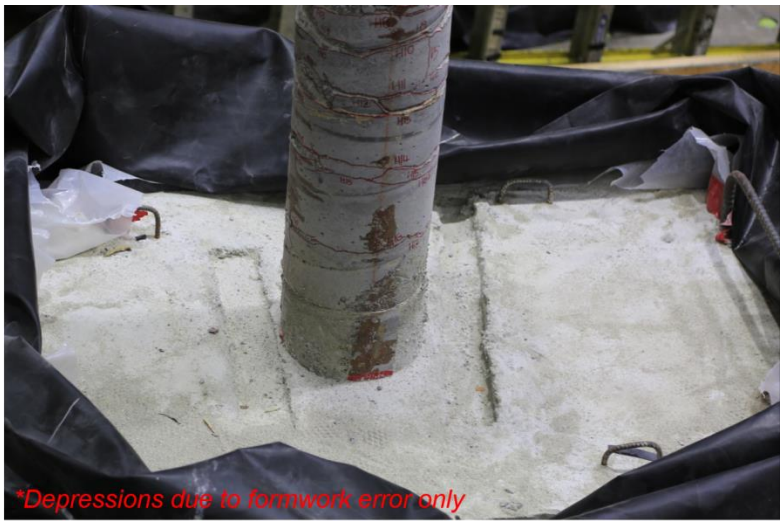

Figure 4-8 Absence of cracks in rock at interface of soils

CHAPTER 5

NUMERICAL SIMULATION OF MODEL SCALE EXPERIMENT

The test specimen was modeled using the finite element software tool Abaqus. Unfortunately, only few soil structure interaction studies exist in literature in which experimental results were successfully replicated using numerical software tools. This task is challenging and matching results have often only been observed for displacements that remained in the linear elastic range. Capturing nonlinear specimen behavior over a large range of displacements poses intrinsic challenges in terms of material behavior (nonlinearity), analysis type (static/dynamic), and computational convergence. The following chapter describes an effort to replicate the global experimental results presented in Chapter 4 and will discuss the challenges and limitations of the analysis.

5.1 Model Description and Geometry

A schematic of the numerical specimen model is depicted in Figure 5-1. The model geometrically replicates an exact copy of the in-situ test specimen. The model includes the test pile and the surrounding soil and rock. The container was not modeled; instead, appropriate boundary conditions were assigned to the FEM model boundaries as explained below.

The test pile consisted of four solid continuum components. The primary component consisted of a solid cylindrical continuum with a length of 3.18m (10.5ft) and a diameter of 25.4 cm (10in). This component represents the overall concrete pile. Within this continuum, three additional components were defined and embedded, namely the #3 longitudinal reinforcement, the #4 longitudinal reinforcement, and the #4 transverse reinforcement (Figure 5-1(c)).

The surrounding soil was modeled as one solid 3D continuum. This combined soil/rock block had dimensions of 1.83m (72in) in length, 1.22m (48in) in width and 2.36m (93in) in height (Figure 5-1(b)). This modeling approach was chosen to omit the challenges associated with assigning interface elements between the rock and soil layer. Instead, a partition was assigned to separate the two layers, and respective material properties could be easily assigned to each layer. The upper 1.34m (53in) of sand were further partitioned to account for varying, depth-dependent soil material properties as shown in Figure 5-1(a).

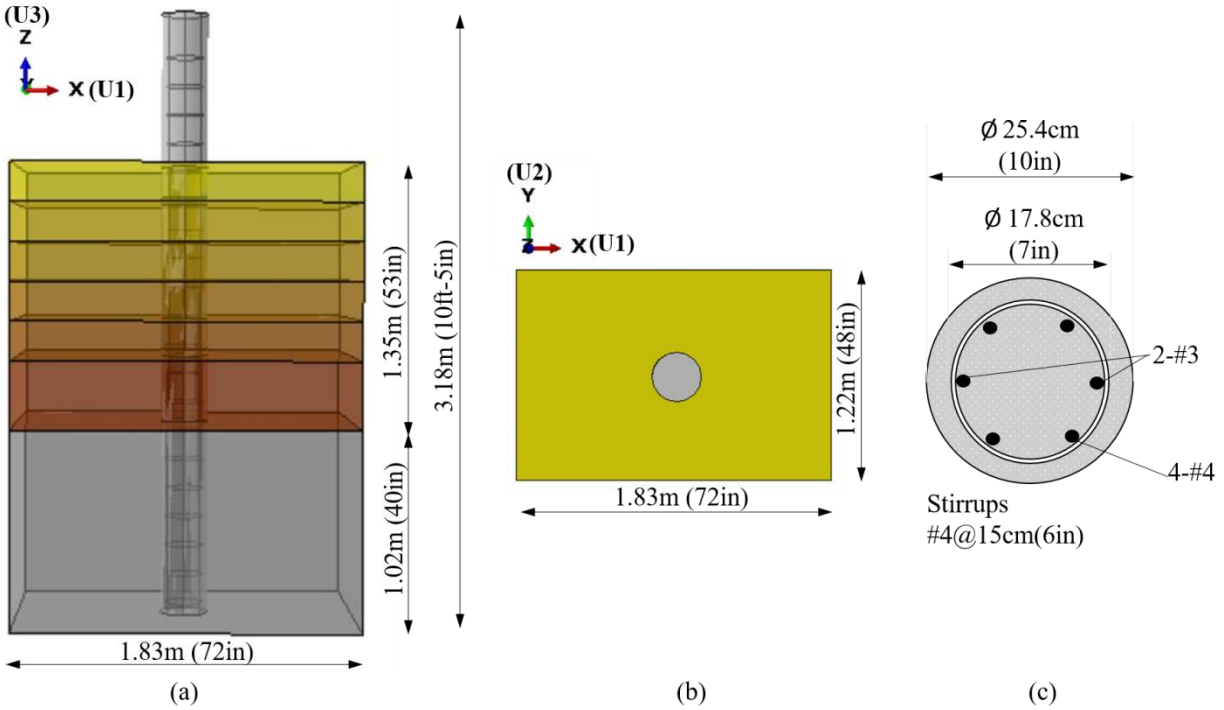

Figure 5-1 Model Geometry Description

5.1.1 Model boundary conditions and component interaction

Displacement and Rotation Constraints

The boundary conditions applied to the pile and soil edges were similar to those utilized in the assessment study. The four outside sides of the soil were restrained in both horizontal directions *X* and *Y*, where *X* is represented by 1 and *Y* is represented by 2 within the Abaqus coordinate system while U is representative of translational displacements. Hence U1=U2=0. The boundaries were not restricted in vertical direction and movement in *Z* direction (U3) were allowed to accommodate potential settlement.

The rock base layer was restricted against any type of displacement, i.e., horizontal, translational and vertical by assigning U1=U2=U3=0. No rotational constraints were specified to any component of the model.

Component Interactions (Pile and Soil)

The surface-to-surface discretization method was employed to model the relative motion between the outer face of the pile and the surrounding soil (sand and rock) surfaces. Similar to

the exercise model described in Chapter 3, the two interaction definitions, i.e., the tangential behavior with finite sliding (friction definition) and the hard contact (pressure overclosure definition) were used to capture the surface interaction. Limited modifications were applied: Instead of the penalty friction algorithm, the friction formulation "Rough" was implemented in the model and showed better computational convergence. This formulation disables any potential slippage between surfaces. Even though this model is computationally more beneficial, it poses a limitation in that it does not allow for separation of materials under applied loading. For loose sand this separation is assumed to be small (as grains fill the voids), however this model is not recommended for cohesive materials where gapping can be significant.

The interaction between the reinforcement steel and the concrete considering bond slip and dowel action is automatically accounted for when using the concrete plasticity model described below. The input parameters are explained in the Section 5.2.

5.1.2 Mesh

Due to the complexity of the model, a simple cubic mesh type was used in the analysis procedure. All solid parts, i.e., pile, sand layers and rock were assigned eight-node cubic elements (C3D8R) with reduced integration. The mesh density was regionally adjusted to capture model nonlinearities and failure evolution.

The pile was longitudinally partitioned into three zones, as illustrated in Figure 5-2(a). The pile-mid region, where plastic hinging was observed during the experiment, was assigned a denser mesh for better convergence in the numerical model. This denser mesh had a mesh size of 30mm (1.2in). The upper and lower part of the pile had a slightly larger mesh size of 50mm (2in).

The soil elements were meshed with cubic C3D8R elements as well. The mesh density was small at the pile-soil interface and increased radially outward. The mesh size near the pile soil interface was 4.5cm (1.8in) and linearly increased to a size of 10cm (3.94in) at the model boundaries. Furthermore, the mesh size was small (4cm, 1.57 in) in the upper layers of soil and gradually increased towards the rock (10cm, 3.94 in). The mesh size was constant across all rock elements. This arrangement showed good degree of sensitivity and computational efficiency. Figure 5-2(b) shows the mesh layout in the soil elements, i.e., the sand and rock.

The steel components were meshed with truss elements. Both the longitudinal and transverse reinforcement are assigned three-node two-dimensional linear truss elements (T3D2) as shown in Figure 5-3 with a mesh size of 15 cm (6 in).

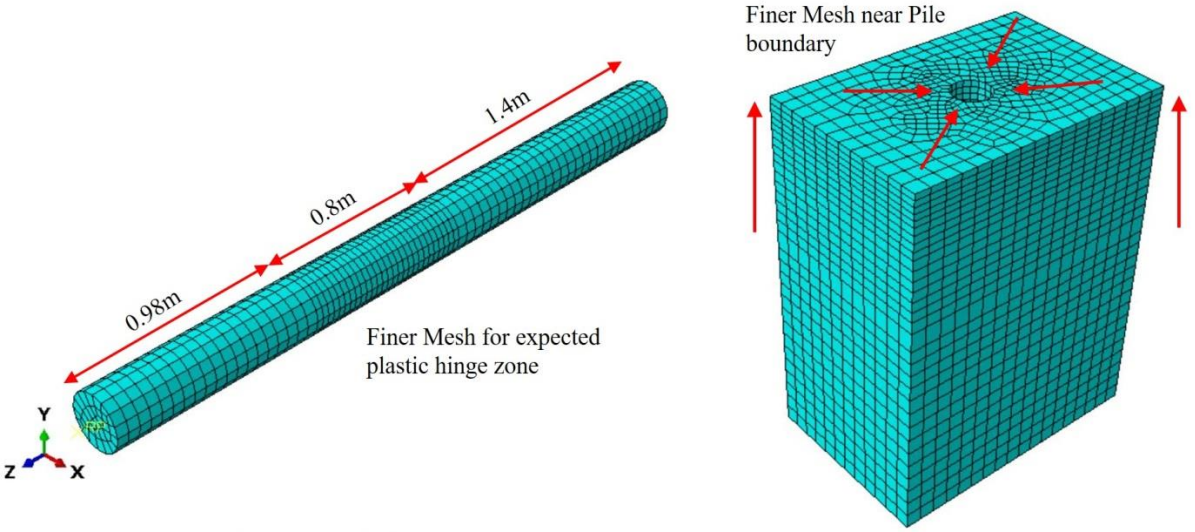

(a) Pile Mesh: 2294 C3D8R Brick elements

(b) Soil Mesh: 8463 elements for Sand; 4030 elements for Rock. C3D8R Brick elements

Figure 5-2 Pile & Soil mesh details

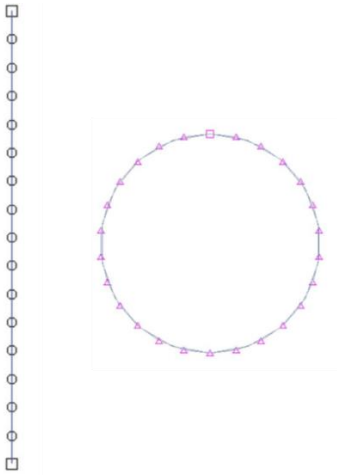

Figure 5-3 Reinforcement Meshes: Linear T3D2 elements

5.2 Material Model Parameters (Constitutive Relationships)

Table 5-1 provides a summary of all model components, dimensions and basic material elasticity parameters.

Table 5-1 Elastic Material Properties of Analysis model

Part	Dimensions	Elastic Material Properties		
		Density (kg/m^3)	**Elasticity** (GPa)	**Poisson Ratio**
Shaft	3.18m x 0.25m diameter (10ft X 10in diameter)	2483	19.7	0.19
Sand	1.83m X 1.22m X 1.34m (72in X 48in X 53in)	1875	(Layered Sand)	0.3
Rock	1.83 m X 1.22m X 1.02m (36in X 24in X 40in)	2000	0.1	0.3
Steel	3.18m (10ft) Longitudinal Stirrups 0.2m (8in) diameter	7850	200	0.3

5.2.1 Soil Model

The sand and rock were modeled using the Mohr-Coulomb failure criterion. Table 5-4 lists the model input parameters for each layer. The sand layer was subdivided into six layers to account for the variation of E-modulus with depth. The upper five layers had a thickness of 20 cm (7.9in), and the bottom layer had a thickness of 34.6cm (13.6in). The E-modulus varied linearly from a very low value (1 MPa, 0.145ksi) in the upper layer to 15MPa (2.17ksi) in the 6^{th} (bottom) layer (Figure 5-4). The rock was assigned an elastic modulus (E_R) of 100MPa (14.5ksi). The resulting stiffness contrast (E_R/E_S) is 6.67. The plasticity parameters for the rock were derived iteratively and fall in the range of typical published material properties for weathered rock (Barton, 1974).

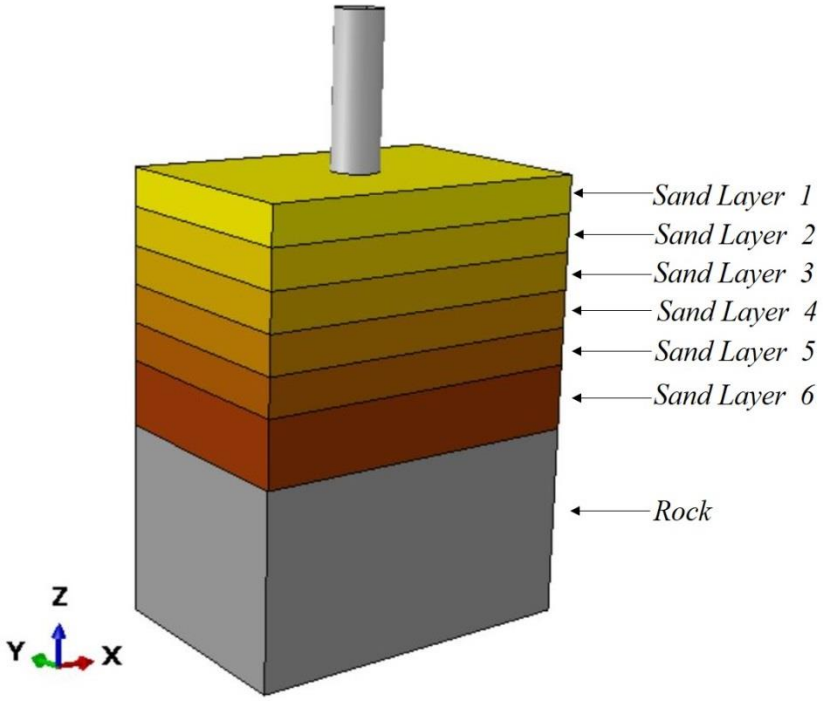

Figure 5-4 Layered Soil Profile

Table 5-2 Soil Plasticity Parameters

Soil Material		Modulus of Elasticity (MPa)	Mohr-Coulomb Plasticity
Sand Layers	1	1	c = 12kPa (1.74psi) ϕ = 37° υ = 0.3 Dil. angle = 3^0
	2	3	
	3	7	
	4	10	
	5	12	
	6	15	
Rock		100	c = 20kPa (2.9psi); ϕ= 43° υ = 0.3; Dil. angle = 3°

Conversion: 1MPa = 145psi

5.2.2 Concrete Damaged Plasticity Model

The concrete was modeled using the concrete damaged plasticity (CDP) constitutive model, a continuum, plasticity-based, damage formulation, most suitable for reinforced concrete elements under monotonic and cyclic loading. The CDP model uses the concepts of isotropic

damaged elasticity in combination with isotropic tensile and compressive plasticity to represent the inelastic behavior of concrete. The design concrete compressive strength for the test pile was 8 ksi (~55MPa). Jankowiak and Lodygowski (2005) conducted extensive tests to identify the correct CDP parameters for class B50 concrete. The parameters recommended by Jankowiak and Lodygowski are used in the computational model and are presented in Table 5-3. The eccentricity, which is related to the material's dilation angle, was changed from 1 to the default value of 0.1. This value assures that the dilation angle remains constant across all magnitudes of confining pressure.

Table 5-3 Concrete Damaged Plasticity Parameters used in FEM Modelling (Jankowiak & Lodygowski, 2005)

CDP Parameters				
Dilation Angle	Eccentricity	$f=f_{b0}/f_c$	K	Viscosity Parameter
38^0	0.1	1.12	0.667	0.0001

Concrete Compression Hardening		**Concrete Compression Damage**	
Stress [MPa]	Inelastic Strain	Damage Parameter	Inelastic Strain
15	0.0	0	0.0
20.197804	0.0000747307	0	0.0000747307
30.000609	0.0000988479	0	0.0000988479
40.303781	0.0001541230	0	0.0001541230
50.007692	0.0007615380	0	0.0007615380
40.23609	0.0025575590	0.195402	0.0025575590
20.23609	0.0056754310	0.596382	0.0056754310
5.257557	0.0117331190	0.894865	0.0117331190

Concrete Tension Stiffening		**Concrete Tension Damage**	
Stress [MPa]	Inelastic Strain	Damage Parameter	Inelastic Strain
1.99893	0.000000000	0	0.000000000
2.842	0.000033330	0	0.000033330
1.86981	0.000160427	0.406411	0.000160427
0.862723	0.000279763	0.69638	0.000279763
0.226254	0.000684593	0.920389	0.000684593
0.056576	0.001086730	0.980093	0.001086730

5.2.3 Steel Model

The reinforcement steel (longitudinal and transverse) was modeled using the plasticity hardening model by Tehrani et al. (1986). This model is appropriate for cyclic loading and has been frequently used in literature to capture tension – compression behavior prior and after material yielding. Wen (2012) developed and calibrated the kinematic hardening parameters for cyclically loaded steel with two back stresses for a Grade 50 steel. Since no material testing for the reinforcement steel was available, these parameters were used for the Abaqus model, even though the yield strength was underestimated by 70MPa (10ksi). The input parameters are summarized in Table 5-4. The steel material was assigned a mass density of 7850kg/m^3 (0.2818pci), a Young's modulus of 200GPa (29000ksi), and a Poisson ratio 0.3.

The steel stress-strain relationship is shown in Figure 5-5. The isotropic hardening behavior of the curves shown in Figure 5-5 can be described using equation 5-1, which formulates the evolution of the yield surface size, σ_0, as a function of the equivalent plastic strain, ε^{pl}. σ_0^y represents the yield stress at zero plastic strain and σ_∞^y & b are material parameters. σ_∞^y is the maximum change in the size of the yield surface.

$$\sigma_0 = \sigma_0^y + \sigma_\infty^y \left(1 - e^{-b\varepsilon^{pl}}\right) \qquad \text{(Eq.5-1)}$$

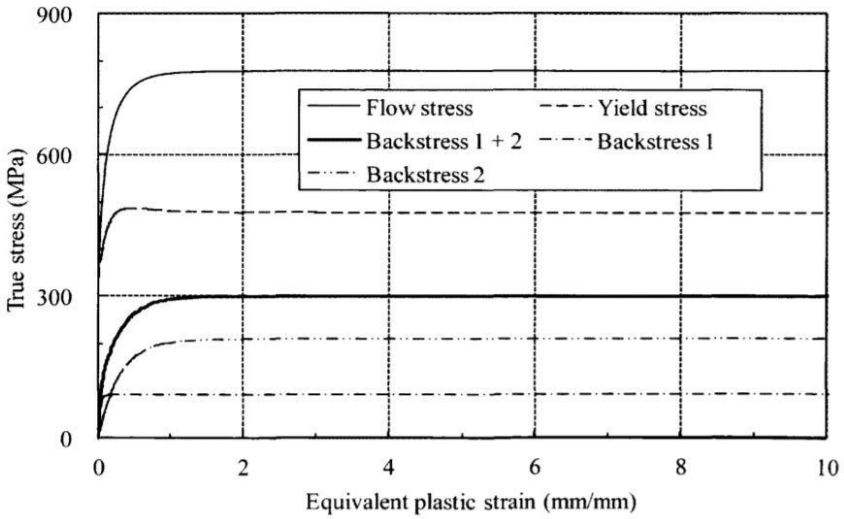

Figure 5-5 Kinematic hardening model - Stress components for tested steel material with two backstresses (Wen, 2012)

Table 5-4 presents the modelling parameters assigned to the steel material in the model. The kinematic hardening parameters consist of a nonlinear kinematic hardening component governed by *C* and an isotropic hardening component governed by γ. *b* defines the rate at which the size of the yield surface changes as plastic straining develops. When the equivalent stress defining the size of the yield surface remains constant ($\sigma_0 = \sigma_0^y$) the model reduces to a non-linear kinematic hardening model. Details of this model can be found in Tehrani et al. (1986) and the Abaqus Documentation.

Table 5-4 Reinforcement steel material modelling parameters

Flow Stress Parameters				**Kinematic Hardening parameters**			
σ_0^y (MPa)	ε_0^p	σ_∞^y (MPa)	b	C_1 (MPa)	γ_1	C_2 (MPa)	γ_2
362	0.0053	417	4.53	3625	39.46	711	3.39

5.3 Load application and loading protocol

Prior to simulating the lateral loading applied during the experimental studies, the gravity loading was defined using initial, geostatic stress conditions. This geostatic stress represents the increase of overburden pressure due to self-weight of the soil and rock materials and was assigned using the 'Predefined Field' option in Abaqus. The vertical stress distribution was calculated in accordance with Eq. 3-4. In a second step, the gravity load of the structural model components (i.e., concrete and steel) was activated. A fixed and automatic time increment was allowed for both analysis steps, respectively.

The lateral load was applied as a static, reverse cyclic load at the pile head. A rigid body tie constraint available in Abaqus' constraint module was specified. A reference point located at a distance of 7.5cm (3in) above the pile head was rigidly tied to the pile head surface as shown in Figure 5-6. The lateral load was applied at that point and engaged the full pile cross-section.

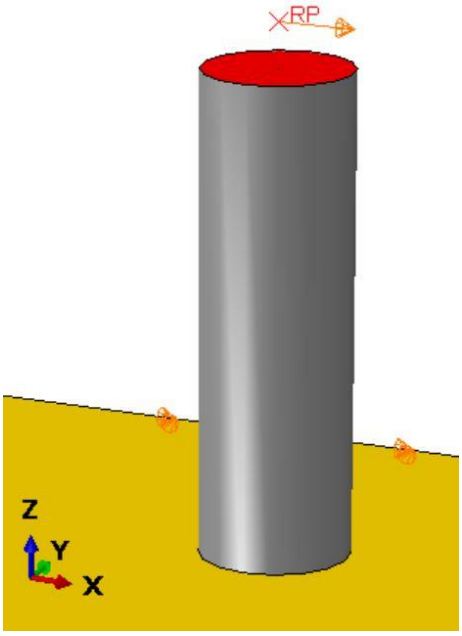

Figure 5-6 Reference Point for Pile Lateral Loading

Figure 5-7 depicts the pile head load history across the 9176 seconds (~2.5 hours) of load application in the laboratory experiment. For simplicity, Figure 5-7 shows the reference axis as fraction of time. Figure 5-7(a) describes the displacement time history applied in the lab. This displacement-time history was used as input displacement into the Abaqus model (i.e. the numerical model was executed under displacement control). Peak displacements recorded during laboratory testing were applied at equal intervals. Figure 5-7(b) shows the corresponding force-time history, which was obtained as result of the numerical analysis. It can be seen that only 1/3 of the loading history could be confidently modeled, hereafter the model did not provide reliable results (i.e., a large error between the numerically obtained and experimental load displacement relationship was observed). This model output is not sufficient to capture the nonlinearity of all model components but provided a preliminary estimate of response profiles due to the applied lateral load. Most literature associates a lateral displacement of 10% of the pile diameter with pile failure. This displacement level (2.5cm, ~1.0in) was achieved in the numerical model.

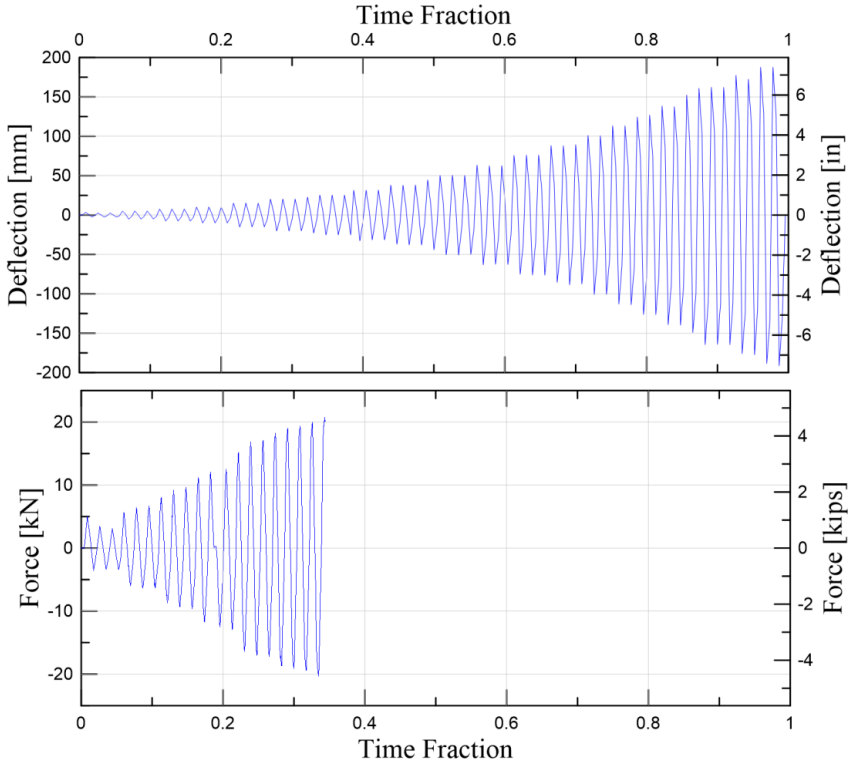

Figure 5-7 (a) Pile head displacement for ABAQUS input and (b) Resulting force time histories

5.4 Results of FEM Analysis

The pile analysis results are presented for a maximum pile head displacement of up to 10% of the pile diameter, i.e., to a lateral deflection of 25mm (1in). The corresponding numerical maximum lateral load was 20.75kN (4.67kips). The pile response profiles were generated using the results of the first cycle at pile head deflection levels of approximately 5mm (0.2in), 10mm (0.4in), 15mm (0.6in), 20mm (0.8in) and 25mm (1in).

5.4.1 Pile deflection profiles

The deflection profiles of the pile under various head displacement levels up to 25 mm is shown in Figure 5-8 from the peaks of each first cycle. The numerical model indicates that all pile displacement occurred within the sand layer. Pile fixity was obtained at a depth of 1.14m (45in) below the sand surface. This depth corresponds to 4.5 pile diameters. No lateral displacement was observed in the rock socket during this level of head displacement. The lateral deflection at the elevation of the sand surface are approximately 50% of the applied pile head deflections.

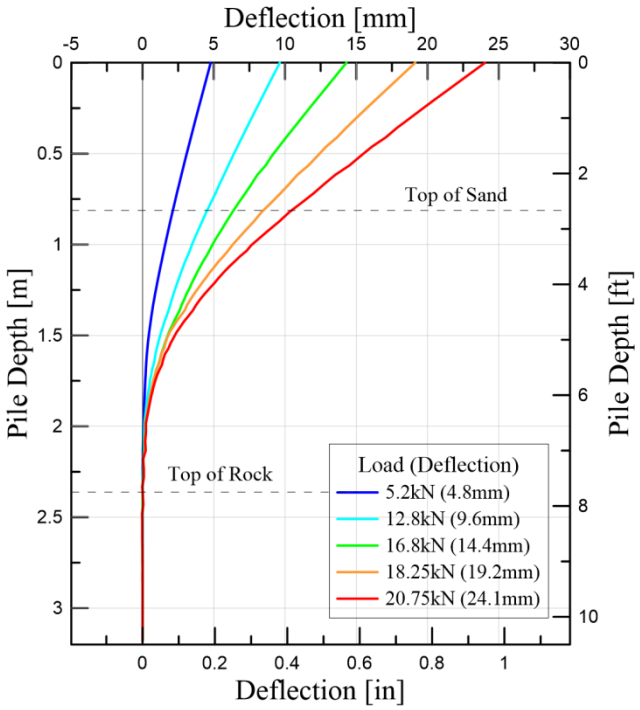

Figure 5-8 Pile Deflection Profile from FEM analysis

5.4.2 Shear and Moment profiles

The internal response profiles for shear, moment and longitudinally distributed stresses were obtained by implementing a dummy element in the pile specimen. This single element with "beam" type profile is used to capture the section behavior as Abaqus does not directly calculate section forces and moments for composite elements such as reinforced piles. This dummy element does not have any structural strength that could influence the structural response behavior of the pile. It can be considered a passive element that solely captures a scaled version of pile forces and stresses. It is only applicable in the linear range of specimen behavior as the bending stiffness *EI* of the dummy element is a reduced scale version of the bending stiffness of the pile. In this case, the sectional rigidity of this beam was 10,000 times smaller than that of the reinforced pile. Once response profile parameters are obtained, the forces and moments measured in the dummy element are scaled back to prototype response quantities.

The numerically obtained shear force and moment profiles are shown in Figure 5-9. The shear force profile indicates the maximum shear force to occur at mid-height within the sand layer. This elevation corresponds to the approximate location of peak moments. With increasing levels of lateral loading at the pile head, the shear forces observed in the analysis showed an

amplification of up to four times of the top lateral load (i.e., 82kN (18.4kips) vs. 20.75kN (4.67kips)). This amplification did not occur at the rock-socket interface as traditionally obtained with the p-y type analysis, but is still larger than anticipated with an FEM type of analysis. Further investigation is required.

Maximum bending moments of up to 32kNm (23.6kip-ft) at 24mm (0.95in) lateral displacements were observed at 0.8m (3.15 pile diameters) below sand surface. As the lateral displacement increased, the peak moment location tends to shift in the upwards direction. The location of the maximum moment during larger displacement cycles coincides with the location of the plastic hinge observed in the experiment.

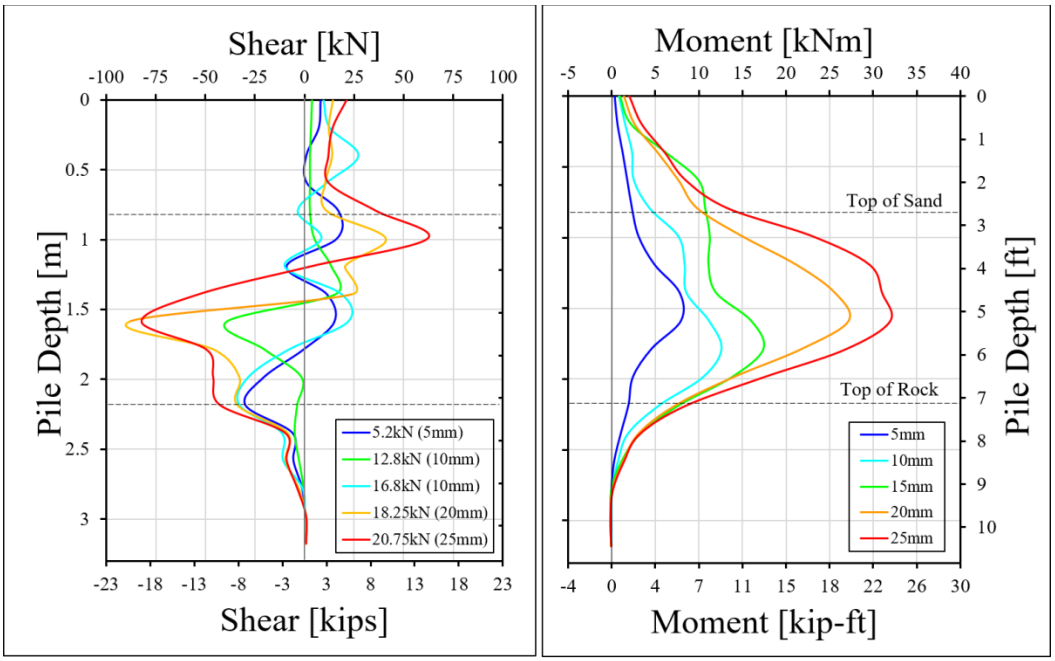

Figure 5-9 Shear & Moment profile from FEM analysis at various head deflections up to 2.5cm.

5.4.3 Stresses in model components

Figure 5-10 (a) to (e) show the progressive stress accumulation in the pile concrete section at various head deflection levels. Within the range of applied displacements, a maximum localized Von-Mises stress of 32.15MPa (4.67ksi) was reached which lead to the development of a critical section within the pile.

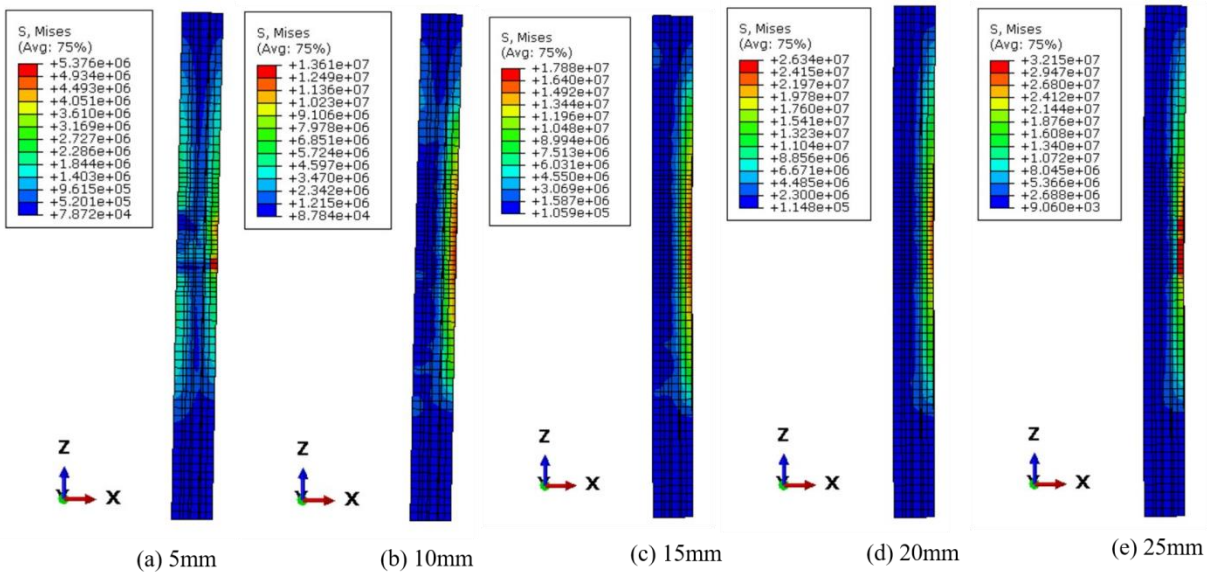

Note: Stresses in Nm^{-2}

Figure 5-10 Section view of Pile Stresses under different pile head deflection

Figures 5-11 (a) to (e) present a similar gradual stress development as shown in Figure 5-10 for the longitudinal reinforcement. The numerically observed peak stress in the outermost steel rebar at a top deflection of 15 mm (0.8 in) was approximately 360MPa (52 ksi) indicating the onset of steel yielding. This corresponds to the assigned material yield strength in the constitutive material model.

Figure 5-12 shows the variation of Von-Mises stresses in the rock and sand layers with respect to depth. For displacement levels less than 10 mm (0.4 in), pile and soil stresses occur at the same side of the pile. As the lateral displacements increase beyond 10mm (0.4in), the stress accumulation in the rock increases, engaging both sides of the pile surface as shown in Figures 5-12 (a) – (e). This indicates the beginning of small pile rotation within the rock socket. The representative color for stresses adapt with the increasing magnitude and become cooler around the rock sockets once rotation has been initiated. The stress variation along depth in the sand shows a stepped profile as a possible result of the stiffness variation in the sand layers.

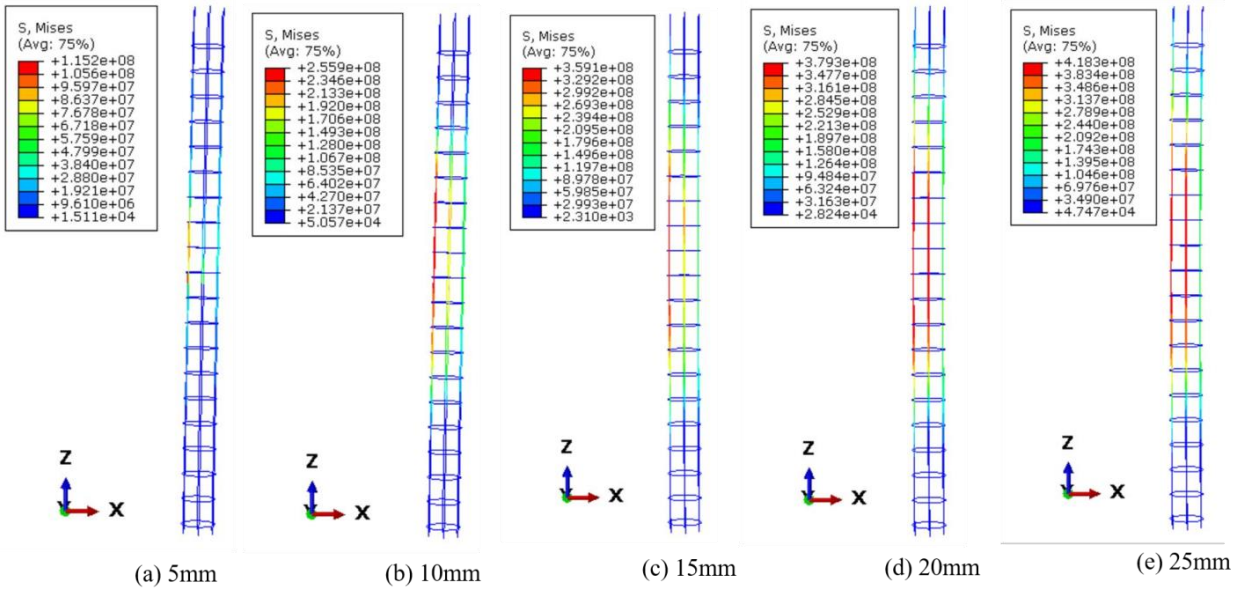

(a) 5mm (b) 10mm (c) 15mm (d) 20mm (e) 25mm

Note: Stresses in Nm^{-2}

Figure 5-11 Stresses in steel reinforcement at different pile head deflections

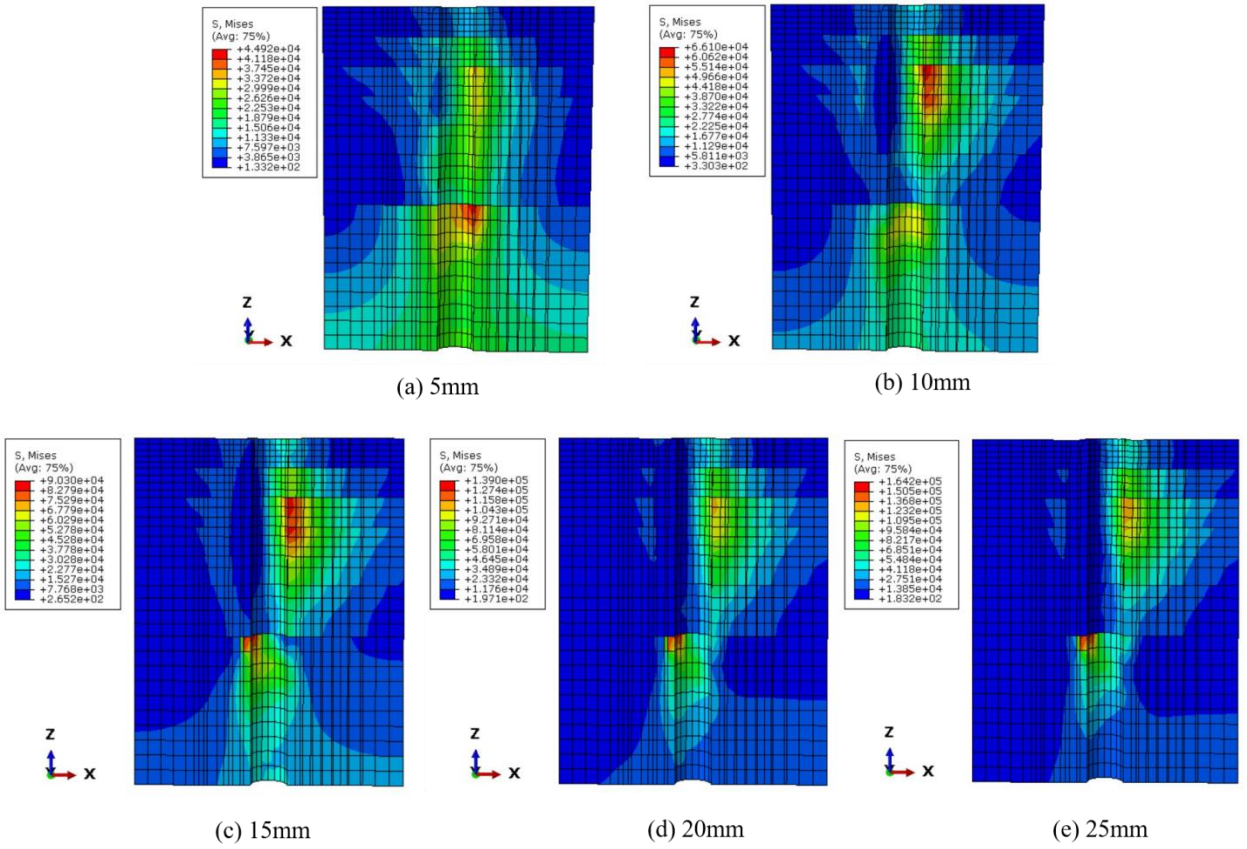

(a) 5mm (b) 10mm

(c) 15mm (d) 20mm (e) 25mm

Figure 5-12 Stress development in sand and rock layers at different pile head deflections

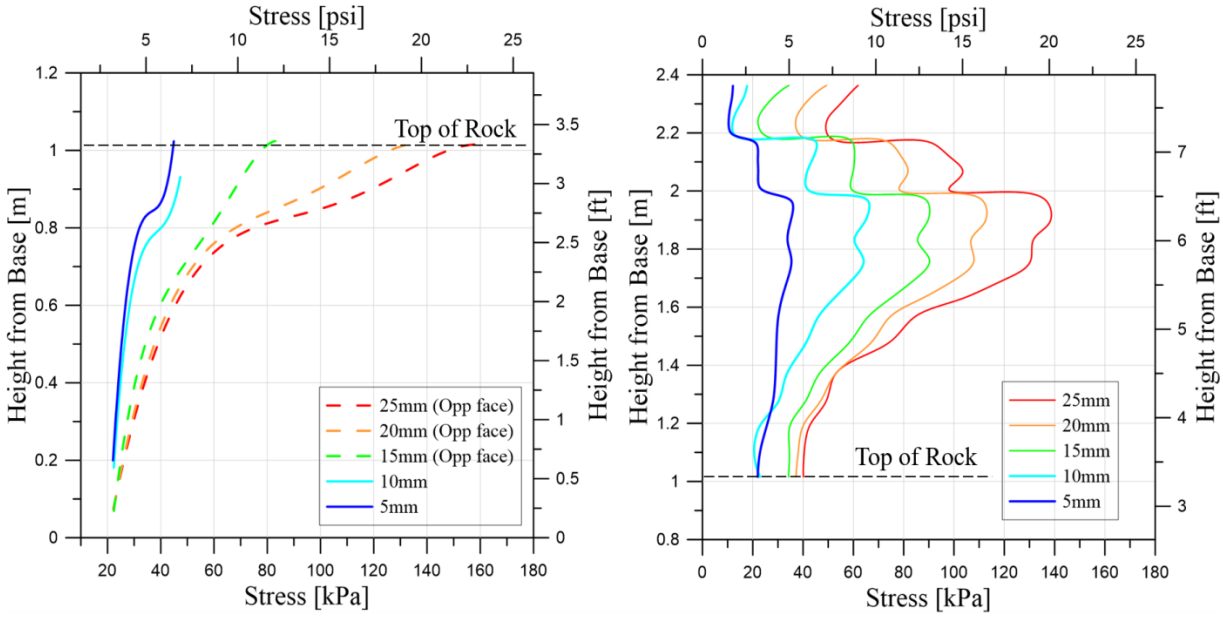

Figure 5-13 Stress profile in Rock & Sand near pile boundary

5.4.4 Plastic hinge development

The results of FEM analysis showed a stress accumulation at pile mid-height. This zone was at a similar elevation as observed in the laboratory test, i.e., approximately 2.5 pile diameters below the initial surface of sand. Following the experiment completion, the pile specimen was excavated and cracking was recorded along the pile length. The documented crack locations fall well within the zone where plastic capacities of the pile were first numerically engaged.

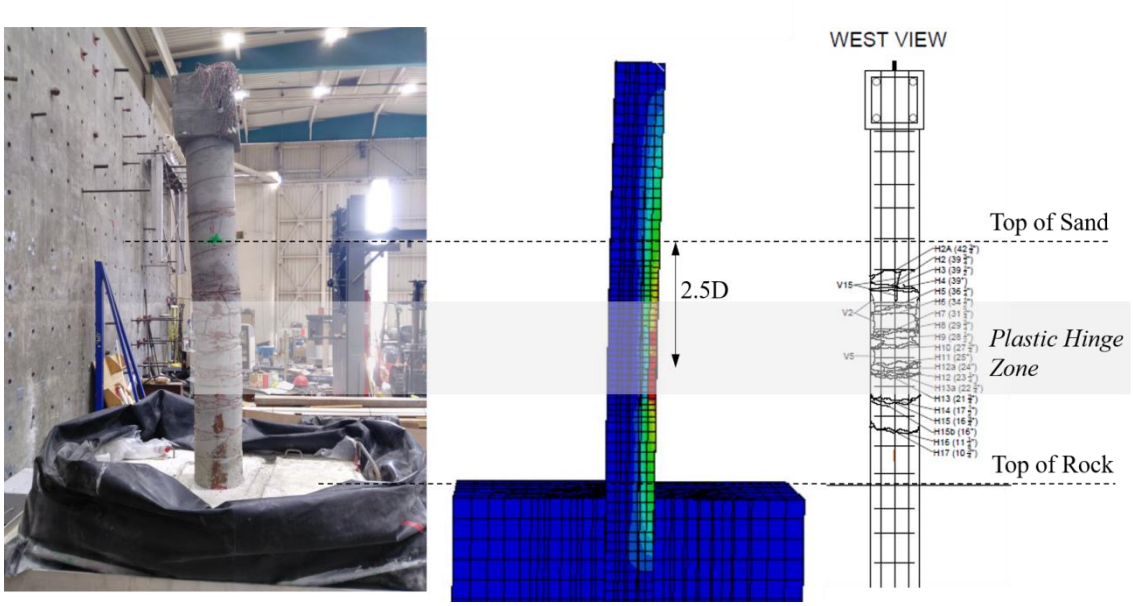

Figure 5-14 Plastic Hinge Zone: Comparison of Test Specimen & FEM analysis

5.4.5 Comparison of experiment and numerical head load displacement relationship

The numerically obtained head load deflection relationship is compared with experimental measurement for a lateral displacement range of up to 25mm (1.0in) and depicted in Figure 5-15. It can be seen that the model response was substantially stiffer than the experimental results and that the loss of specimen stiffness was not captured well, even though appropriate material relationships were implemented. The initial stiffness was overestimated by 45% in the FEM model. The ultimate capacity was overestimated across all lateral displacement levels by about 30%. Figure 5-16 extrapolates the numerical results to an even larger displacement level, where model-experiment discrepancies become strongly apparent. Even though the model reached the maximum lateral load level at a displacement of 25mm (1.0in), no softening was observed in the model results. Hence this load displacement response is not well captured. This discrepancy could be attributed to an overestimation of soil stiffness that prevents a larger accumulation of lateral deflections along the pile length.

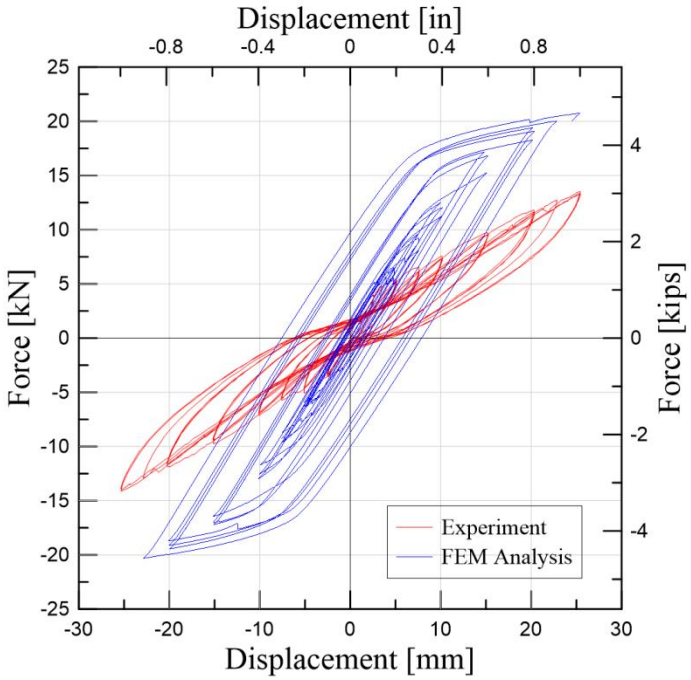

Figure 5-15 Force-displacement comparison of experimental data and FEM analysis up to deflections equivalent to10% of the pile diameter

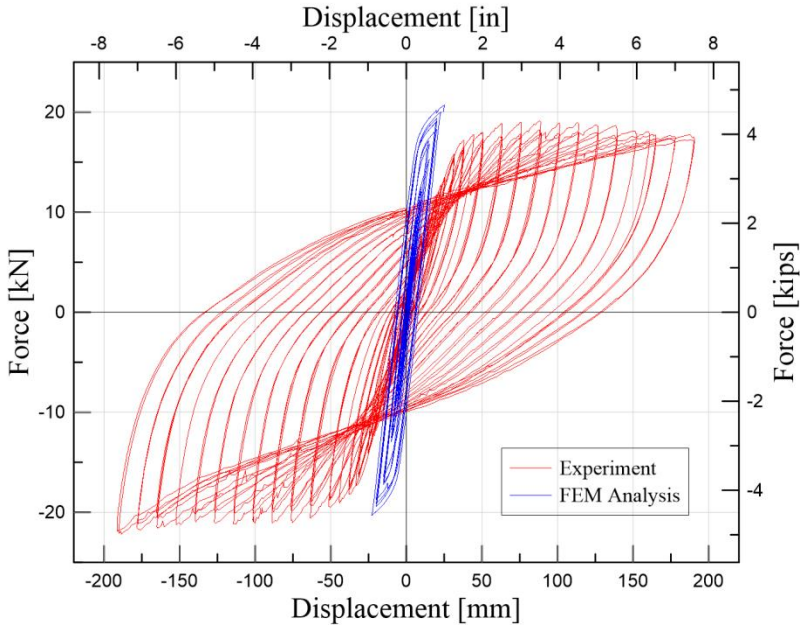

Figure 5-16 Overall force-displacement comparison of experimental data and FEM analysis

CHAPTER 6

SUMMARY AND RECOMMENDATIONS

This thesis presents results of an experimental-numerical research study conducted on a 25.4 cm (10in) diameter model-scale, reinforced concrete, rock-socketed pile under lateral cyclic loading. For piles in soil strata with substantial stiffness contrasts (i.e. weak surface layer on top of strong bottom layer), internal pile demands, such as pile shear and pile bending moments, are key demand parameters that influence the structural design and constructability of the deep foundation element. Specifically, the amplification of shear forces near the rock-socket interface is recognized among the geotechnical engineering community as controversial design aspect and has been treated in various forms, by either designing for this amplification, or by ignoring this amplification in the specification of transverse reinforcement. In preparation of a large-scale testing program on rock-socketed drilled shafts, the model scale results and numerical analysis presented in this document serve as preliminary study to investigate the global nonlinear behavior and to verify the test setup and specimen instrumentation.

This thesis first reviews a series of experimental and numerical studies conducted on deep foundations embedded or socketed in rock. Hereafter, the results of a model scale lateral load test are presented. The following key points summarize the experimental setup and specimen behavior observed in the laboratory. Additional details can be found in Favaretti (2018).

a. A reinforced concrete, free head pile with a slenderness ratio of 12 was embedded in a simulated “rock”. The pile concrete compressive strength was 55 MPa (8ksi) reinforced with 1.3% longitudinal steel and transverse reinforcement adequate for 195kN (44kips) of shear force. The rock consisted of 27 MPa (4ksi) compressive strength concrete. The pile was socketed across an embedment length of 1.02 m (40in). The overlaying sand layer had a height of 1.34m (53 in). The stiffness contrast between the rock and sand layer was $E_R/E_S = 6.67$.
b. The pile was cyclically loaded up to a displacement of 70% of the pile diameter. Loading was applied at the pile head through a hydraulic actuator. Loading consisted of quasi static reverse cyclic displacement levels. Specimen yielding was observed at a deflection

of 3.3cm (1.3in), which corresponds to 13% of the pile diameter. The corresponding yield load was recorded to be 16kN (3.6kips).

c. Significant displacement in the upper layer of sand was observed. The maximum moment and plastic hinge in the pile was formed at a distance of approximately 2.6 pile diameters below the initial surface of sand. No displacement or cracks were observed in the pile or the rock near the rock–soil boundary. The strength of the pile concrete was twice the compressive strength of the concrete simulating the "rock". This can be used as a situation depicting a strong pile socketed in a weak or weathered rock.

The laboratory experiment was simulated using the software platform ABAQUS to further study the specimen response via finite element modeling. The pile concrete and reinforcing steel adopted constitutive models suitable to capture the material behavior under cyclic loading conditions. The Mohr-Coulomb plasticity criterion was used to configure the bedrock and overlying sand. The model parameters were iteratively derived until appropriate pile response behavior was obtained. Key findings of the FEM study are summarized below.

a. A simulation of load displacement relationships and pile response profiles up to a lateral head deflection of 10% of the pile diameter was conducted. The yield load in the numerical analysis was found to be 25-30% higher than the experimentally recorded load. The initial stiffness of the load displacement curve was found to be 30% higher than the experimental stiffness. The model was not able to reach deformations larger than 10% of the pile diameter without introducing a substantial mismatch between prescribed displacements and forces. Hence the full nonlinear behavior up to large levels of lateral displacements was not replicated.
b. The numerical pile response agreed well with the damage evolution observed in the test. The areas of high stress numerical concentrations within the pile coincided with the plastic hinge location recorded after pile excavation.
c. The numerical analysis of stress propagation in the sand layer revealed that even though a lateral spacing of three pile diameters between the pile and soil laminar box was provided, the boundaries of the experimental system (i.e., walls of the laminar container) were engaged and likely contributed to the overall stiffness of the pile-soil system.

d. Similar to experimental observations, the simulated rock did not experience very large stress concentrations. This indicates that pile demands resulting from shear and moment were effectively transferred along the pile and into surrounding soil layers.
e. A numerical shear amplification was noticeable in the region of pile failure. The numerical magnification was up to four times of the applied lateral load at pile head. For lower lateral load levels, the pile exhibited a highly varying shear profile which could potentially result from the combined effect of cyclic loading and differential soil stiffness throughout the depth of the sand.

The overall comparison of the FEM analysis with the tested specimen showed an acceptable level of coherence. The findings of the analysis serve as basis for the future large-scale testing program for laterally loaded piles. Some recommendations arising from this research exercise and its findings are suggested below:

a. The stiffness contrast between the rock and the soil (E_R/E_S) can be further increased to intensify the effects of shear magnification and shear transfer to the bedrock.
b. Various levels of transverse reinforcement ratio should be considered (i.e., from insufficient reinforcement, to minimal code reinforcement, to adequate reinforcement).
c. An improvement in the finite element modelling scheme can reveal potential zones of pile failure which can be assessed for varying transverse volumetric steel ratios. This improvement can be with respect to detailed analysis of concrete specimens (uniaxial compression, uniaxial tension and triaxial tests as well as point load bending tests) along with cyclic load tests on reinforcing steel to obtain crucial parameters necessary for the respective constitutive models.
d. Additionally, soil behavior can be modelled with results from more accurate laboratory tests such as the triaxial tests under appropriate confinement and drainage conditions. The soil parameters obtained from these tests should be implicated in an advanced constitutive model (e.g. Drucker Prager (CAP) Plasticity) which are better able to capture complex soil behavior under dynamic loading conditions. Furthermore, these finite element models should be calibrated using the right

boundary conditions with the performed laboratory material tests before confidently applying them to full-scale experimental analyses.

e. The model must be assessed for proper gap formations between the pile and the surrounding soil once the loose soft layer has been displaced in the vicinity of the pile. Gaps were not allowed to form in the current model and may have contributed to the misfit between experimental and numerical results. Convergence issues associated with the separation after contact in the pressure overclosure definitions have to be better understood to allow for reduction in the area of contact between the pile and the upper layers of sand during the load reversal cycles.

f. A minimum spacing of five pile diameters in the loading direction is recommended for the future large scale testing.

REFERENCES

ABAQUS Theory Guide 6.14. (2014). *Dassault Systèmes Simulia Corp.* Providence, Rhode Island, USA.

Abdel-Mohti, A., & Khodair, Y. (2014). Analytical investigation of pile-soil interaction in sand under axial and lateral loads. *International Journal of Advanced Structural Engineering*, 6-54.

Agah-Tehrani, A. E. (1986). *The Theory of Elastic-Plastic Deformation at Finite Strain with Induced Anisotropy Modeled as Combined Isotropic-Kinematic Hardening.* Troy, NY: Metal Forming Report, Rensselaer Polytechnic Institute.

Barton, N. (1974). A review of the shear strength of filled discontinuities in rock. *Norwegian Geotech. Institute, Oslo*, Publ. No. 105.

Brown, D., & Shie, C.-F. (1990). Three Dimensional Finite Element Model of Laterally Loaded Piles. *Computers & Geotechnics 10*, 59-79.

Carter, J. P., & Kulhawy, F. H. (1992). Analysis of Laterally Loaded Shafts in Rock. *Journal of Geotechnical Engineering, Vol. 118, No. 6*, 839-855.

Chehadeh, A. S. (2014, June). Analysis and Design of Circular Shafts Using Finite Element Method. *Masters Thesis*. Sharjah, UAE: American University of Sharjah.

Cho, K., Clark, S., Keaney, B., Gabr, M., & Borden, R. (2011). Laterally loaded drilled shafts embedded in soft rock. *Transportation Research Record 1772*, 3-11.

Dykeman, P., & Valsangkar, A. (1996). Model studies of socketted caissons is soft rock. *Canadian Geotechnical Journal*, 747-759.

Ensoft, Inc. (2004). *User's Manual for LPILE.*

Favaretti, C. (2018). Model scale tests on laterally loaded piles in sand. *Doctoral Dissertation*. Irvine: University of California, Irvine.

Frantzen, J., & Stratten, W. (1987). *Final Report: p-y curve data for laterally loaded piles in shale and sandstone, Rep. No. FHWA-KS-87-2.* Topeka, Kansas: Kansas Department of Transportation.

Gabr, M., Borden, R., Cho, K., Clark, S., & Nixon, J. (2002). *P-y curves for laterally loaded drilled shafts embedded in weathered rock.* FHWA/NC/2002-08, North Carolina Department of Transportation.

Guo, F., & Lehane, B. (2016). Lateral response of piles in weak calcareous sandstone. *Canadian Geotechnical Journal, 53(9)*, 1424-1434.

Hetenyi, M. (1946). *Beams on Elastic Foundations.* Ann Arbor: Universtity of Michigan Press.

Hoek, E., & Brown, E. (1988). The Hoek-Brown criterion – a 1988 update. *15th Canadian Rock Mechanics Symposium: rock engineering for underground excavations,* (pp. 31-38). University of Toronto.

Jankowiak, T., & Lodygowski. (2005). Identification of Parameters of Concrete Damage Plasticity Constitutive Model . *Foundations of Civil And Environmental Engineering, No. 6*, 53-69.

Kahle, K. J., & Brown, D. A. (2002). *Performance of Laterally Loaded Drilled Sockets Founded in Weathered Quartzite.* Alabama: Highway Research Center & Harbert Engineering Center, Auburn University .

Kulhawy, F., & Phoon, K. (1993). Drilled shaft side resistance in clay soil to rock. *Design and performance of deep foundations: Piles and piers in soil and soft rock, ASCE,* 172-183.

Liang, R., Yang, K., & Nusairat, J. (2009). p-y Criterion for Rock Mass. *Journal of geotechnical and geoenvironmental engineering*, 26-36.

LPILE^{TM}. (2010). A Program for the Analysis & Design of Piles and Drilled Shafts Under Lateral. Austin, Texas: Ensoft, Inc. Engineering Software.

Parsons, R. L., Pierson, M. C., Willems, I., Han, J., & Brennan, J. J. (2011). Lateral Resistance of Short Socktets in Weak Rock: a Case History. *Transportation Research Record: Journal of the Transportation Research Board, No. 2212*, 34-41.

Poulos, D., & Davis, E. (1980). *Pile analysis and design. Series in Geotechnical Engineering.* New York: John Wiley & Sons Inc.

Poulos, H. (1971). Behavior of Laterally Loaded Piles. I: Single Piles. *Journal of Soil Mechanics & Foundations Div., ASCE,* 711-731.

Randolph, M. (1981). The response of flexible piles to lateral loading. *Geotechnique, 31(2)*, 247-259.

Randolph, M., Dolwin, R., & Beck, R. (1994). Design of driven piles in sand. *Geotechnique, 44*, 427-448.

Reese, L. (1984). FHWA-IP-84-11. In *Handbook on Design of piles and drilled shafts under lateral load.* Washington D.C.: Federal Highway Administration, US Dept. of Transportation.

Reese, L. C. (1997). Analysis of Laterally Loaded Piles in Weak Rock. *Journal of geotechnical and geoenvironmental engineering*, 1010-1017.

Reese, L., & Matlock, H. (1956). Non-dimensional solutions for laterally loaded piles with soil modulus assumed proportional to depth., (pp. 1-23). Austin, Texas.

Trochianis, A., Bielak, J., & Christiano, P. (1988). A three-dimensional non-linear study of piles leading to the development of a simplified model. 8-176. Department of Civil Engineering, Carnegie Institute of Technology.

Turner, J. (2006). *Rock-Socketed Shafts for Highway Structures Foundations.* Washington D.C.: National Cooperative Highway Research Program - Synthesis 360.

Vu, T. T. (2006). Laterally Loaded Rock Socketed Drilled Shafts. *Doctoral Dissertation*, . University of Wyoming.

Wang, S., & Reese, L. (1993). COM624P - Laterally Loaded Pile Analysis Programfor the Microcomputer. Version 2.0. *Federal Highway Administration Publication No. FHWA-SA-91-048* .

Wen, Z. (2012, May). Modelling of Ductile Fracture in Steel Structures for Monotonic & Cyclic Loading. *Doctoral Thesis*. Ottawa, Ontario: Department of Civil & Environmental Engineering, Carleton University.

Yang, K. (2006, May). Analysis of Laterally Loaded Drilled Shafts in Rock. *Doctoral Dissertation*. University of Akron.

Yang, K., & Liang, R. (2006). Methods for deriving py curves from instrumented lateral load tests. *Geotechnical testing journal*(30 (1)), 31-38.

Yu, H., & and Houlsby, G. (1991). Finite Cavity expansion in dilatant soils: loading analysis. *Geotchnique, 41(2)*, 173-183.

Yuan, S., Zhang, K., Liu, Z., & Li, J. (2014). Numerical Tests on laterally loaded drilled shafts in socketed rock. *Advanced Materials Research Vols. 919-921*, 706-709.

Zhang, L., Ernst, H., & Einstein, H. (2000). Nonlinear analysis of laterally loaded rock-socketed shafts. *Journal of Geotechnical and Geoenvironmental Engineering. v.126 issue 11*, 955-968.

Zhang, L., Silva, F., & Grismala, R. (2005). Ultimate lateral resistance to piles in cohesionless soils. *Journal of Geotechnical and Geoenvironmental Engineering, v.131 No.1*, 78-83.